Springer Proceedings in Materials

Nizar Meksi
Sonia Dridi-Dhaouadi
Ibtissem Moussa *Editors*

Proceedings of the 4th International Congress of Applied Chemistry and Environment (ICACE–4)

Advances in Chemistry and Clean Processes on Materials

Springer

Springer Proceedings in Materials 97

Springer Proceedings in Materials publishes the latest research in Materials Science and Engineering presented at high standard academic conferences and scientific meetings. It provides a platform for researchers, professionals and students to present their scientific findings and stay up-to-date with the development in Materials Science and Engineering. The scope is multidisciplinary and ranges from fundamental to applied research, including, but not limited to:

- Structural Materials
- Metallic Materials
- Magnetic, Optical and Electronic Materials
- Ceramics, Glass, Composites, Natural Materials
- Biomaterials
- Nanotechnology
- Characterization and Evaluation of Materials
- Energy Materials
- Materials Processing

To submit a proposal or request further information, please contact one of the following Springer Publishing Editors according to your affiliation location:

European countries: **Mayra Castro** (mayra.castro@springer.com)
India, South Asia and Middle East: **Swati Meherishi** (swati.meherishi@springer.com)
South Korea: **Smith Chae** (smith.chae@springer.com)
Southeast Asia, Australia and New Zealand: **Ramesh Nath Premnath** (ramesh.premnath@springer.com)
The Americas: **Michael Luby** (michael.luby@springer.com)
China and all the other countries or regions, as well as topics in materials chemistry: **Maggie Guo** (maggie.guo@cn.springernature.com)
This book series is indexed in **SCOPUS** and **EI Compendex** database.

Nizar Meksi · Sonia Dridi-Dhaouadi ·
Ibtissem Moussa
Editors

Proceedings of the 4th International Congress of Applied Chemistry and Environment (ICACE–4)

Advances in Chemistry and Clean Processes on Materials

Springer

Editors
Nizar Meksi
Textile Engineering
National Engineering School of Monastir
Monastir, Tunisia

Ibtissem Moussa
Higher Institute of Technology Studies
of Ksar Hellal Environmental Chemistry
and Clean Processes Laboratory
University of Monastir
Monastir, Tunisia

Sonia Dridi-Dhaouadi
Preparatory Institute for Engineering Studies
of Monastir
University of Monastir
Monastir, Tunisia

ISSN 2662-3161 ISSN 2662-317X (electronic)
Springer Proceedings in Materials
ISBN 978-981-95-4187-4 ISBN 978-981-95-4188-1 (eBook)
https://doi.org/10.1007/978-981-95-4188-1

This Springer imprint is published by the registered company Springer Nature Singapore Pte Ltd.
The registered company address is: 152 Beach Road, #21-01/04 Gateway East, Singapore 189721, Singapore

Preface

The 4th International Congress of Applied Chemistry and Environment (ICACE-4) took place from December 12 to 14, 2024, in Tozeur, Tunisia. This congress was organized by the Laboratory of Environmental Chemistry & Clean Processes (LCE2P–Faculty of Sciences, University of Monastir, Tunisia), co-organized with ATuTeD (Tunisian Association of Sustainable Technologies), and held in partnership with the Laboratory of Thermal and Thermodynamics of Industrial Processes (L2TPI–National Engineering School, University of Monastir, Tunisia). This event provided an excellent opportunity for researchers, academics, and industrial partners to present their work and engage in fruitful exchanges.

These proceedings bring together up-to-date research findings, innovative methodologies, and emerging technologies. They reflect the congress's mission to promote collaboration between academia, research institutions, and industry, as well as to foster creativity and innovation in the fields of chemistry, environment, and sustainable development.

We sincerely thank all authors, reviewers, and participants whose contributions made ICACE 2024 a success. We would like to give special recognition to the organizing committee, keynote speakers, and session chairs for their dedication and commitment in creating a stimulating and productive academic environment.

We hope that the knowledge shared and discussions held at ICACE 2024 will inspire further research, foster new collaborations, and advance the fields of applied chemistry and environmental technologies for the benefit of society.

Ibtissem Moussa
Nizar Meksi
Sonia Dridi-Dhaouadi

Committees

Conference Chair

Hatem Dhaouadi	Faculty of Sciences of Monastir, Tunisia

President of the Scientific Committee

Nizar Meksi	National School of Engineering of Monastir, Tunisia

President of the Organizing Committee

Ibtissem Moussa	Higher Institute of Technology Studies of Ksar Hellal, Tunisia

Organizing Committee

Sonia Dridi	Preparatory Institute of Engineering Studies of Monastir, Tunisia
Imene Ghezal	Higher Institute of Technology Studies of Ksar Hellal, Tunisia
Wafa Ghedira	Faculty of Sciences of Monastir, Tunisia
Noureddine Baaka	Higher Institute of Fashion of Monastir, Tunisia
Amira Zgolli	Faculty of Sciences of Monastir, Tunisia
Maha Abdelileh	National Engineering School of Monastir, Tunisia
Maryi Teieb	Faculty of Sciences of Monastir, Tunisia
Monia Chaabane	National Engineering School of Monastir, Tunisia
Nizar Kerekni	Faculty of Sciences of Monastir, Tunisia
Siwar Majdoub	Biotechnology Center of Sfax, Tunisia
Ghazza Masmoudi	Faculty of Sciences of Monastir, Tunisia
Imen Chermiti	Faculty of Sciences of Monastir, Tunisia

Scientific Committee

Ahmed Bellagi	National School of Engineers of Monastir, Tunisia
Chedly Boudokhane	Faculty of Pharmacy of Monastir, Tunisia
Mohamed Farouk Mhenni	Faculty of Sciences of Monastir, Tunisia
Zine Mighri	Faculty of Sciences of Monastir, Tunisia
Adel Ghith	National School of Engineering of Monastir, Tunisia
Amel Babay	Higher Institute of Technological Studies of Ksar-Hellal, Tunisia
Aminoddine Hajji	Yazd University, Iran
Ayoub Haj Said	Microelectronics and Nanotechnology Research Center of Sousse, Tunisia
Boubaker Jaouachi	National School of Engineering of Monastir, Tunisia
Faouzi Sakly	Higher Institute of Technological Studies of Ksar-Hellal, Tunisia
Faten Fayala Guith	National School of Engineering of Monastir, Tunisia
Hatem Majdoub	Faculty of Sciences of Monastir, Tunisia
Hatem Mhiri	National School of Engineers of Monastir, Tunisia
Heikki Seppä	University of Helsinki, Finland
Houcine Barhoumi	Faculty of Sciences of Monastir, Tunisia
Khaled Boughzala	Higher Institute of Technological Studies of Ksar-Hellal, Tunisia
Latifa Bergaoui	National Institute of Applied Sciences and Technology, Tunisia
Marie-Odile Simonnot	University of Lorraine, France
Mohamed Ben Hassen	Higher Institute of Technological Studies of Ksar-Hellal, Tunisia
Mohamed Hamdaoui	National School of Engineering of Monastir, Tunisia
Mohamed Hassen V. Baouab	Preparatory Institute for Engineering Studies in Monastir, Tunisia
Mustapha Majdoub	Faculty of Sciences of Monastir, Tunisia
Néji Ladhaari	Higher Institute of Fashion of Monastir, Tunisia
Rafik Gharbi	Faculty of Sciences of Monastir, Tunisia
Sabria Barka	Higher Institute of Biotechnology of Monastir, Tunisia
Saber Ben Abdessalem	National School of Engineering of Monastir, Tunisia
Saoussem Hammami	Faculty of Sciences of Monastir, Tunisia
Salah Akkal	University of Mentouri Constantine 1, Algeria

Sonia Dridi-Dhaouadi	Preparatory Institute of Engineering Studies of Monastir, Tunisia
Taoufik Harizi	Higher Institute of Fashion of Monastir, Tunisia

Contents

Environment

About the Editors

Dr. Nizar Meksi

is a professor at the National School of Engineers of Monastir (University of Monastir, Tunisia) in the Department of Textile Engineering. He also works as a researcher at the Laboratory of Environmental Chemistry & Clean Processes (LCE2P) of the Faculty of Sciences of Monastir (University of Monastir, Tunisia). He graduated in 2000 from the National School of Engineers of Monastir in the specialty of Textile Chemistry, before obtaining two Master's degrees (2001 and 2003) from the University of Lille 1 and the University of Littoral, France. Then, he completed a PhD in Chemistry (2009) at the Faculty of Sciences of Monastir. Finally, in 2014, he obtained the Postdoctoral Qualification (Habilitation) in Textile Engineering from the University of Monastir.

His research interests focus on the development of novel cleaner processes in the textile industry, the chemical modification and grafting of textile polymers, as well as microencapsulation and its applications. Particular attention is given to the use of life cycle assessment (LCA) methodology to evaluate the environmental impacts of the developed durable processes. During his career, he designed and coordinated several research projects with industry and supervised various postgraduate students. He has been a member of scientific committees, organizing committees, and has participated in national and international evaluation boards.

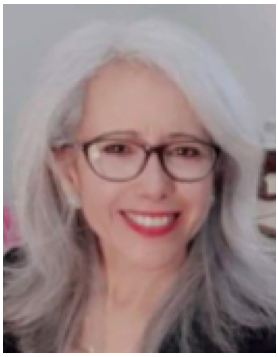

Sonia Dridi-Dhaouadi

is a professor of Chemistry at the Preparatory Institute for Engineering Studies of Monastir (Tunisia) and a member of the Laboratory of Environmental Chemistry and Clean Processes (LR21ES04). She holds a PhD in Process Engineering from INPL–ENSIC Nancy, France (1997) and a Habilitation to Supervise Research in Chemistry from the University of Monastir (2012).

Her research focuses on water pollution treatment by adsorption, the valorization of solid wastes into activated carbons, eco-friendly textile dyeing, and life cycle assessment of industrial processes. As the coordinator of several national and international research projects, she has

developed innovative processes, including textile dyeing in supercritical CO_2.

She is the author of numerous scientific publications, a holder of multiple patents, and supervises PhD and master's students in her fields of expertise. Her commitment also extends to academic project management, participation in capacity-building initiatives, and the evaluation of collaborative research programs.

Dr. Ibtissem Moussa

is an assistant professor in the Department of Textile Engineering at the Higher Institute of Technological Studies of Ksar-Hellal (University of Monastir, Tunisia) and a member of the Environmental Chemistry & Clean Processes Laboratory (LR21ES04) at the Faculty of Sciences (University of Monastir, Tunisia). She obtained her engineering diploma in Textile Chemistry from the National Engineering School of Monastir (ENIM) in 2013 and earned her PhD in Textile Engineering from the same institution in 2018.

Her research focuses on the valorization of agricultural and industrial by-products for the development of eco-friendly materials and biopolymers. She specializes in the extraction and application of natural dyes for intelligent textiles and color-indicator fabrics. Her work emphasizes sustainable processes and circular economy strategies.

She is the author of numerous peer-reviewed publications and patents. She has actively participated in organizing committees, serving as president of one, and has been involved in national and international research project committees.

Renewable Energie and Climate Change

Investigation of a Solar Powered Ejector Absorption Cooling System Under Tunisian Climatic Conditions

Doniazed Sioud[1](✉), Raoudha Garma[2], and Ahmed Bellagi[1]

[1] Energy Engineering Department, Ecole Nationale d'Ingénieurs de Monastir, ENIM, University of Monastir, Monastir, Tunisia
siouddoniazed@gmail.com

[2] Physics Sciences Department, Ecole Supérieure des Sciences et de La Technologie de Hammam Sousse, University of Sousse, Sousse, Tunisia

Abstract. In this paper, investigate a solar absorption cooling system is theoretically investigated. A Linear Fresnel Solar Concentrator drives a combined ejector single effect absorption cycle. High performance is comparable to double effect absorption cycle in the combined ejector single effect absorption, which require driven temperatures higher than single-effect ones. A mathematical model of the collector concentrator is represented to analyze its optical performance. Simulations are conducted to examine the performance of the combined absorption cycle COP_{cycle}, instead of studying the entire machine performance COP_{system}. Simulations are carried out for a generator driving temperature and pressure of 180 to 230 and 198 to 270 kPa, respectively. A case study in cooling season, during summer typical Tunisian day, showing how cycle and system performance are affected by sun radiation and surrounding temperature, are investigated. Simulation results show that collector efficiency is between 0.54 and 0.78 and that COP_{system} and COP_{cycle} reach minimum values at 14:00, about 0.7 and 0.45 respectively.

Keywords: Solar cooling · combined absorption system · linear Fresnel collector

1 Introduction

All over the world there is a high energy demand, especially in hot weather region such as Mediterranean cities because of the important demand of cooling and air conditioning particularly in the spring and summer periods, for buildings and industrial processes in both small and high scale. Thus this holds a significant part of energy consumption in buildings which necessitates, due to the actual energy emergency, quick steps must be taken to lower energy expenses and their negative environmental effects.Government and researches deal with the use of solar cooling technologies as an attractive solution. A 250 kW thermal prototype utilizing a Fresnel concentrator [1] was studied both theoretically and experimentally. Results demonstrated that thermal effectiveness per day was greater than 40%.Tests of a solar/gas cooling plant at Seville in Spain was done during

N. Meksi et al. (Eds.): ICACE 2024, SPM 97, pp. 3–8, 2025.
https://doi.org/10.1007/978-981-95-4188-1_1

2008–2009 [2]. The technology of Fresnel concentrator, in another industrial process was studied like an integrated multi-effect device and solar building concentrated power station [3]. Five Algerian coastline locations were analyzed using dynamic model, using TRNSYS 17 software However the main disadvantages vast regions of collectors if the double effect absorption cycle is used, and limited efficiency of solar powered devices ones single-effect absorption chillers is adopted. Some modified configurations, such ejector single effect cycle [4, 5], which requires a high temperature heat source and has a double effect cycle efficiency due to the integration of an ejector between before the condenser. In this paper, a solar combined single effect system is studied. So a Linear Fresnel collector is used to produce high temperature flow able to produce steam in high temperature to drive the generator. The effect of driving chilled water and inlet cooling water temperatures on the overall system and on the ejector absorption cycle performance's, respectively COP_{system} and COP_{cycle} are performed. Additionally, a study of a specific case of an ordinary summer day is studied.

2 System Description

A linear Fresnel collector connected to an ejector single effect system using LiBr-H_2O represents the solar cooling system under study, presented in Fig. 1 While the adopted Linear concentrating Fresnel collector (IS-LF11) [6] have surface of 136 m^2. In the objective of producing driving steam at higher temperature ranging from 180 °C to 230 °C to drive the generator of the cooling machine, to drive one unit of the combined LiBr-H_2O absorption chiller to produce cooling temperatures in the range of 12 °C to 4 °C were simulated.

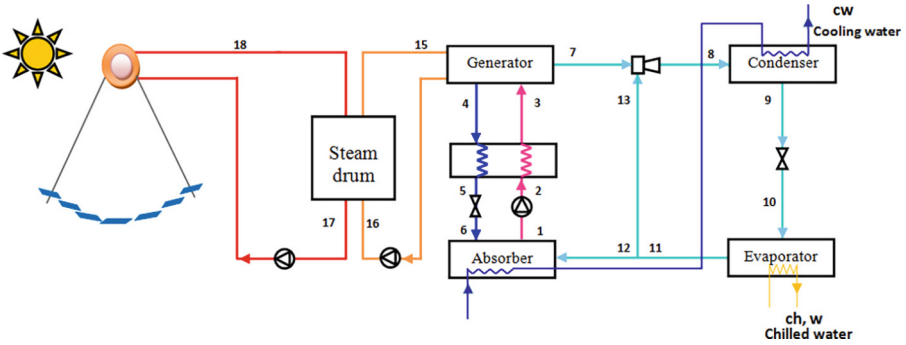

Fig. 1. Solar ejector absorption single effect system.

3 Mathematical Model

3.1 Model of Linear Fresnel Collector

Optic performance is characterized via a correction factor defined as (IAM) which is the incidence angle modifier, taken in account to determinate the Optical performance for different angle of incidence, which should be multiplied with η_0. With ΔT is the

difference between surrounding air and heat transfer flow HTF, temperatures:

$$\Delta T = T_{HTF} - T_{amb} T^2 \tag{1}$$

In second order, the primary reflector's thermal losses per square meter is as follows:

$$\dot{q}_{loss} = u_0 A_{aperture} \Delta T + u_1 A_{aperture} \Delta T^2 \tag{2}$$

The collector's useful heat source depends on both thermal loss and optical performance, calculated as below:

$$\dot{q} = \eta_{optical}\,(\alpha, \theta)_{\delta} G.A - \dot{q}_{loss}(\Delta T) \approx \eta_0 IAM_l(\theta_{l,\delta}).IAM_t(\theta_{t,\delta}).A.G - u_1.A.\Delta T^2 \tag{3}$$

Using the approximation of the optical performances (efficiency) which is represented by the factored bidirectional IAM projected transversally and longitudinally on zenith angles, respectively θ_t and θ_l.

The ratio of useable thermal energy to the solar irradiation gathered is provided by the collector's thermal efficiency, or η.

$$\eta \approx \eta_0 IAM_l(\theta_{l,\delta}).IAM_t(\theta_{t,\delta}) - u_1.A.\frac{\Delta T^2}{G} \tag{4}$$

When the sun is at its zenith, and both equal 1.

3.2 Combined Ejector Single Effect Absorption Cycle Model

For the purposes of simulating the performance of this particular absorption system, the principles of mass and energy conservation are used. This absorption system COP is defined as:

$$COP_{cycle} = \frac{\dot{Q}_e}{\dot{Q}_{steam,g} + \sum \dot{W}_P} \tag{5}$$

4 Results and Discussions

The combined ejector single effect absorption refrigeration cycle coupled with the liner Fresnel collector was thermodynamically analyzed using a computer model built with the Engineering Equation Solver (EES) software [7]. The total coefficient of performance is a crucial metric for characterizing the whole system performance COP_{system} of a solar ejector-absorption refrigerator. The collector efficiency (η) multiplied by the combined refrigeration cycle coefficient of performance COP_{cycle}, yields the total COP_{system} of the solar absorption system, which is defined as follows [8]:

$$COP_{system} = \eta.COP_{cycle} \tag{6}$$

4.1 Chilled Water Temperature Effects on System and Cycle Efficiencies

For different inlet chilled water temperature, driving temperature impacts in the overall cycle and on the performances of the combined absorption machine is represented in Fig. 2, if the cooling fluid is at 32 °C. So first, the COP increases when the driving temperature rise and decrease with the increase of the chilled water temperature.

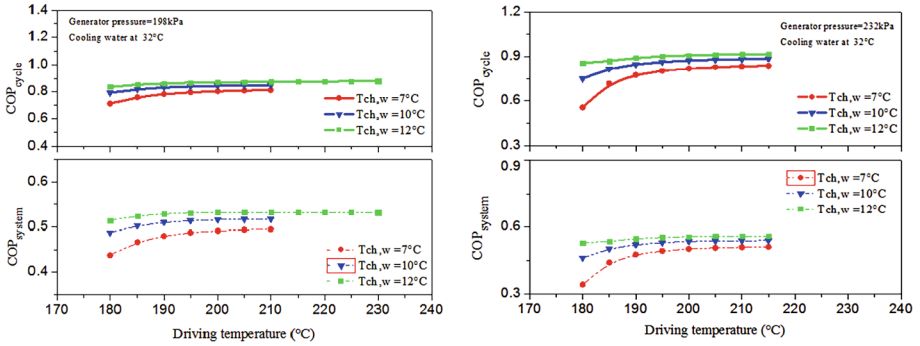

Fig. 2. Effect of driving and chilled water temperature on the COP vs., generator pressure set at (a) 198 kPa and (b) 232 kPa.

4.2 Case Study According to Hourly Local Data

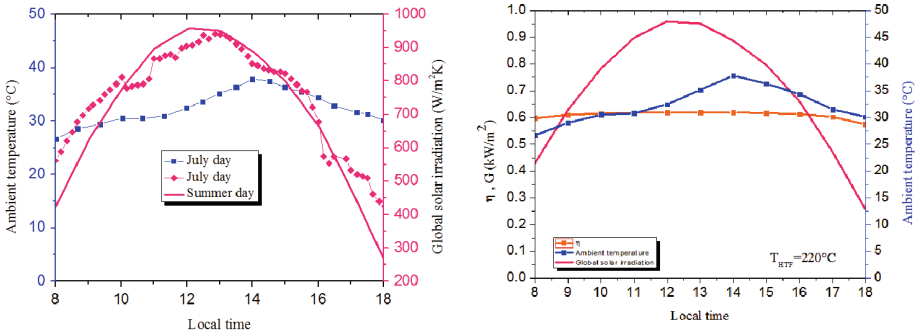

Fig. 3. **(a)** Evolutions of the solar irradiation and the surrounding temperature in a July typical summer day, in Tunisia, ref [9], **(b)**, and Linear Fresnel efficiency of the collector vs., solar irradiation and surrounding temperature as heat transfer flow temperature is fixe.

In July 2008, [9] conducted a thermal check of weather and solar conditions. An example of (16 July 2008) day in the northern Tunisian capital, which has a Maritime environment defined by abundant sun energy, is depicted in Fig. 3(a). The tested region is situated at latitude 36° and longitude 10°. With 350 clear days annually. The temperature

of the surrounding air is therefore ranges from 27 °C to 39 °C, and the solar radiation is at least 250 W/m^2 and exceeds 900 W/m^2. At 12:00, the maximum sun radiation is 958 W/m^2. At 14:00, however, the highest recorded ambient temperature is 37 °C. The Linear Collector employed in the simulations had an average efficiency of around 0.6 for normal summer day (Fig. 3 (a)) and a highest value of 0.62 (Fig. 3 (b)). The efficiency of the collector as explained above (model collector) and Eq. (5) relies on the temperature differential among the surrounding temperature and the heat transfer flow, which is quadratic. Therefore, rather than the irradiation G, the efficiency of the collector is influenced by the working values of T_{HTF}. Thus, when the heat transfer flow temperature is less, collector efficiency is higher, as shown in Fig. 4. Also as illustrated in Fig. 3(a), because of the varying patterns of solar radiation and the surrounding temperature between 11:00 and 15:00, the collector efficiency is specifically higher at this period than the rest of the day, as represented in Fig. 4.

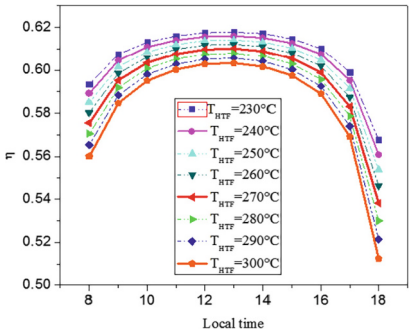

Fig. 4. Collector efficiency during one day for different HTF temperatures.

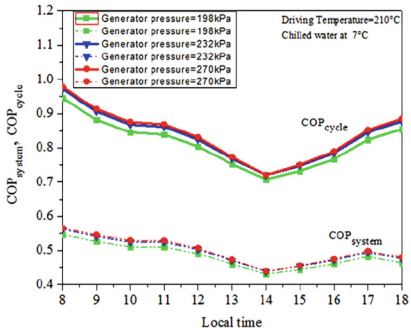

Fig. 5. COP_{system} and COP_{cycle} at local time for different pressure in the generator.

Figure 5 shows the evolution COP_{system} and COP_{cycle} along the operating period of the local time, reach levels greater than 0.7 at all frequently. Both COP variation decrease with increasing the ambient temperature, that is why the curves have the reciprocate trend

of the ambient temperature curve. Therefore, they reach a minimum when the ambient temperature is in the highest point mean at hour 14:00.

5 Conclusion

A solar cooling combined ejector single effect absorption system is proposed and investigated. Steam condensation ranges from 180 °C to 230 °C power the refrigerator studied, via heat from the pressured water from Linear Fresnel Collector that coupled the combined single effect cycle. A case study of typical summer day is studied. According to the analysis, the Linear Collector employed in the simulations had an average efficiency of around 0.6 and a maximum efficiency of 0.62. Also it is found that the collector efficiency depends on the temperature differential between the ambient temperature and the heat transfer flow that is quadratic. So both temperature of the working values of T_{HTF} and the irradiation G affect the collector efficiency. When the temperature of the heat transfer flow is less, the collector efficiency is higher.The evolution COP_{system} and COP_{cycle} along the operating period of the local time, reach levels greater than 0.7. Both performance variations decreases with increasing the surrounding temperature.

References

1. Hani, B., Djaffar, S., Christophe, L., Noureddine, S.: Theoretical and experimental performance analysis of a Fresnel type solar concentrator. Renew. Energy **101**, 782–793 (2017)
2. Pablo, B., Francisco, J.P., Felipe, R.: Solar absorption cooling plant in Seville. Sol. Energy **84**, 1503–1512 (2010)
3. Mohammed, L., Driss, N., Djamel, O.: Analysis of the feasibility of combined concentrating solar power with multi effect desalination for Algerian coast. Int. J. Renew. Energy Res. 782–793 (2017)
4. Sun, D.W., Eames, I.W., Aphornratana, S.: Analysis of a solar operated ejector absorption refrigeration system. Int. J. Refrig **19**(3), 172–180 (1996)
5. Aphornratana, S., Eames, I.W.: Experimental investigation of a combined ejector-absorption refrigerator. Int. J. Energy Res. **22**, 195–207 (1998)
6. Industrual Fresnel web
7. . Christine, W., Michael, B., Florian, M., Alexander, H., Tomas, N.: Solar cooling with water-ammonia absorption chillers and concentrating solar collector-operational experience. Int. J. Refrig. **39**, 57–76 (2014)
8. Klein, S.A., Alvarado, F.: Engineering Equation Solver. F–chart software, Middleton (2003)
9. Balghouthi, M., Chahbani, M.H.: Investigation of a solar cooling installation in Tunisia Author links open overlay panel. Appl. Energy **98**, 138–148 (2012)

Trombe Wall Optimised for Mediterranean Climate: An Architectural Strategy for Energy Efficiency

Marwa Ammar[1(✉)], Nahed Soussi[1], Ameni Mokni[1], Hatem Mhiri[1], and Philippe Bournot[2]

[1] Laboratory of Thermal and Thermodynamic of Industrial Processes, Road of Ouardanine, National School of Engineers of Monastir, 5000 Monastir, Tunisia
ammarmriwa@gmail.com
[2] Aix Marseille Univ, CNRS, IUSTI, Marseille, France

Abstract. Since buildings make a major contribution to the distribution of total energy, it is essential to take into account their functionality and the repercussions this has. Passive solar technology is a vital part of contemporary architecture, and the Trombe wall, as one of its principles, certainly stands out from the others.

The new transparent Trombe wall (T-T-W) can receive solar intensity from all four sides. We developed the addition of parallel slats of transparent insulating material (TIM-PS) in the newly designed T-T-W with the help of a numerical study using CFD simulation. Taking the actual climatic conditions of a winter solstice day with a Mediterranean climate, the optimal design of a T-T-W was investigated. The use of perpendicular TIM-PS can eliminate convective heat loss through the south glass wall, increasing thermal efficiency from less than 5% to over 19% at 17H.The operating time when the TIM-PS is placed increases from 9 h for the conventional glass wall to 11 h for the perpendicular glass wall equipped with TIM-PS. This high-performance design ensures high thermal comfort, even at the lowest levels of sunlight, guaranteeing good thermal comfort in the early hours of the night. Nevertheless, adjusting the slats on the south-facing glass wall would not reduce the amount of incident radiation, as the slat material, polymethyl methacrylate (PMMA), is highly transmissive (92%).

Keywords: CFD · Trombe Wall · Slats · Transparent insulation material

1 Introduction

Trombe walls are a passive solar heating system that utilizes a thick wall, typically painted black, to absorb and store solar heat, which is then gradually released into a building. This system is particularly effective in reducing heating costs and enhancing thermal comfort in buildings, making it a sustainable architectural solution. The design and efficiency of Trombe walls can vary significantly based on factors such as climate, wall configuration, and materials used. Recent studies have explored various configurations and enhancements to improve their performance, including the use of thermal fins, phase

N. Meksi et al. (Eds.): ICACE 2024, SPM 97, pp. 9–16, 2025.
https://doi.org/10.1007/978-981-95-4188-1_2

change materials (PCMs), and multi-duct systems. These innovations aim to optimize heat transfer and storage, thereby increasing the overall thermal efficiency of Trombe walls.

Trombe walls can be configured with thermal fins to enhance heat transfer. A study found that a configuration with three fins at a 70° rotation angle achieved the highest thermal efficiency, while five fins oriented horizontally were optimal at low Reynolds numbers (Alaoui et al., 2024). [1].

The use of PCMs in Trombe walls can significantly enhance energy storage and thermal comfort by absorbing and releasing heat more effectively ("Modeling and analysis of energy and exergy performance of a PCM-augmented concrete-based Trombe wall systems", 2023).[2].

Multi-duct Trombe walls, which incorporate tubular solar collectors, have shown improved thermal efficiency and heating capacity compared to traditional designs (Li et al., 2024). [3].

Trombe walls can reduce heating demands by up to 33% in certain climates, although they may increase cooling demands during warmer months (Bogdanovic et al., 2018) [4].

In cold climates, Trombe walls can significantly improve indoor thermal comfort, with studies showing temperature increases of up to 14 °C in the air channel and a maximum thermal efficiency of 84%(Hernández-Pérez et al., 2025) [5].

The use of inert gases in the air gap of a Trombe wall can enhance system efficiency by up to 20.6% compared to air (Alaoui et al., 2024). [1].

While Trombe walls offer significant energy savings, their effectiveness can be limited by factors such as low solar radiation in winter and potential overheating in summer (Dong et al., 2024) [6].

The initial cost and complexity of design can pose challenges, particularly when integrating advanced materials and configurations (Patel, 2024) [7].

Despite their benefits, studies on the current situation and challenges of Trombe wall optimization are limited; Trombe walls face challenges such as the need for precise design to avoid overheating and the initial costs associated with advanced configurations. However, ongoing research and technological advancements continue to enhance their feasibility and performance, making them a promising solution for sustainable building design. It is therefore necessary to provide improvements in Trombe wall architecture to ensure optimized Trombe wall performance.

For this reason, we opted firstly to increase the transmitting surface of solar radiation, and secondly to reduce convective losses to the outside. To achieve this, we came up with a new design for the Trombe wall with transparent side faces and roof, as well as transparent slats attached to the transparent south face of the Trombe wall.

Numerical simulation analyses of energy performance, on an hour-by-hour basis, were carried out using the ANSYS software in order to analyze the performance of an innovative Trombe wall design. The new innovative design is designed to receive solar radiation from all four sides, during the entire daily sunshine period in winter, thus reducing convective losses to the exterior.

2 Numerical Model

2.1 Simulation Procedures

The Trombe wall was analyzed using ANSYS FLUENT 16.1 software, leading to accurate predictions on future design. It is believed that the flow is incompressible, turbulent, and regular. The continuity, momentum, and energy equations that form the basis of the airflow model are solved for a three-dimensional Cartesian system.

The time frame between 6 a.m. and 6 p.m. was considered during the simulation.

To arrive at this answer, the whole discretization process relied on high-precision models. Because of natural convection, the solution relies on pressure and uses a pressure-velocity coupling technique. The set of fundamental equations was closed using the popular standard k-model.

The SIMPLE model was used for spatial discretization of pressure, whereas the second-order upwind model was used for momentum, turbulent kinetic energy, turbulent dissipation rate, and energy.

The DO radiation model and a solar calculator for Mediterranean climate at a certain time of day and year were used to implement the impact of radiation.

3 Description of Simulated Model of Trombe Wall

Based on an architectural perspective, it's critical to make sure there is enough natural light, as well as suitable panoramic views and cozy environment. Compromises must frequently be made when designing. Which materials and concepts may be used depends on the site's geographic and climatic features. A mix of different materials and concepts is made possible by the variety of materials that may be used, the ways in which they can be employed, the environment, and the circumstances of construction.

Although Trombe Wall system's are auxiliary and cannot independently keep the building at a consistent temperature, they can aid in lowering the amount of energy used for heating. The Mediterranean climate zone is the target of the design.

With many façades exposed to the wind and natural ventilation, the structure is regarded as a separate family house.

Both the Trombe wall and the simulated structure's energy simulation were examined. If the climate in a Mediterranean location is examined, heavy, huge constructions may be able to lower the energy required for heating and cooling.

The study was conducted using a model of a south-facing structure with one story, around $9m^2$ of functional space, and 25 m^3 of volume Fig. 1. The experimental light cell is located in Abha, Asir, Saudi Arabia, with a Mediterranean climate; its latitude and longitude are 18.23°N and 42.66°E, respectively. The Trombe wall is typically constructed using blocks of masonry or concrete; within this lightweight structure, it is built with 70-mm-thick panels of wood. Inside the wooden room, the Styropor material is used for insulation. A transparent 6 mm thick glazing is located 400 mm in front of the massive wall and has a high transmittance. In this Trombe wall, different from classic TW, lateral walls of the air gap zone are same as the south façade; made by transparent 6 mm thick glazing, to allow the maximum amount of solar flux to enter the Trombe wall zone. After passing through the glass, the solar radiation strikes the Trombe wall and

heats it up. Heat is transferred from the outside to the inside of the wall by conduction. The rate at which heat transfers through the Trombe wall depends on the material it is made of and its thickness.

To optimize energy efficiency, position it toward the south (in the northern hemisphere).

A transparent Trombe wall was first designed experimentally, then validated using a numerical study. In a second phase, this research focused on an innovative Trombe wall comprising parallel slats of transparent insulating material attached to the southern glass wall. A special Trombe zone is defined in the space between the glass and the wall, and comprises transparent insulating material in the form of parallel slats. The wall is connected to the main zone as an inner surface. Natural convection takes place in the air space of the classic Trombe wall. Regardless of the low outside temperature, the sun's rays passing through the glass heat the solid wall structure.

The glazing, which covers a large part of the exterior surface of the south wall, represents the zone through which the greatest convective heat loss occurs, so adding transparent insulation material in this area will help reduce it Fig. 2.

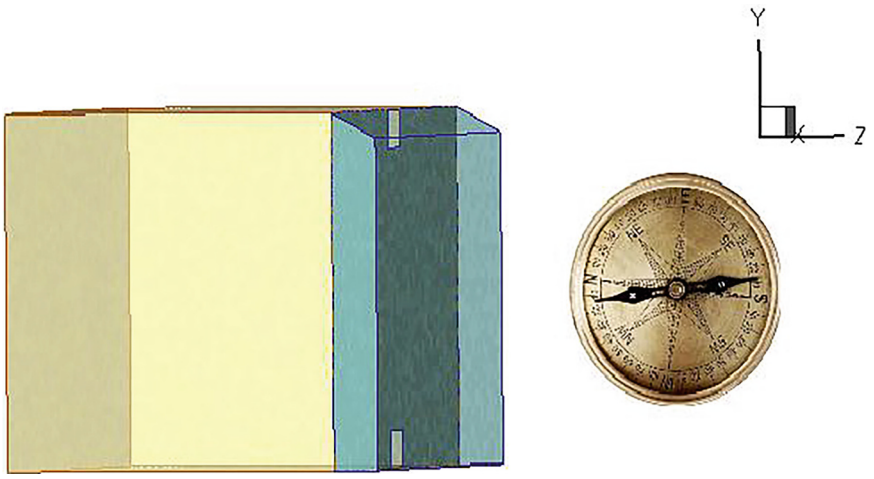

Fig. 1. The Transparent Trombe Wall in 3D Model

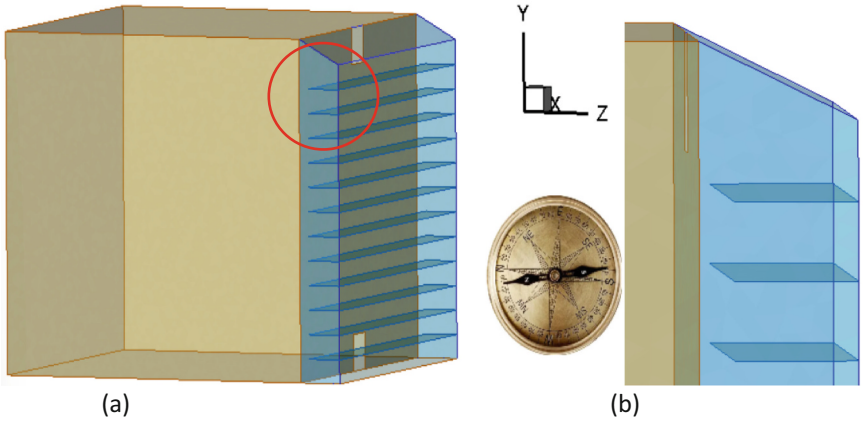

Fig. 2. A **(a)** 3D Model of the transparent Trombe wall including 12perpendicular TIM-PS, **(b)** zoomed view TIM-PS.

4 Results and Discussion

4.1 Thermal Efficiency of T-TW with TIM-PS

Designers must have a thorough understanding of climate factors because strategies of energy-efficient passive design largely depend on meteorological factors. The efficiency of this system can significantly fluctuate. The Trombe wall system is particularly beneficial in Mediterranean climates. Fewer energy systems are needed and there is less fuel consumption, which means there are benefits.

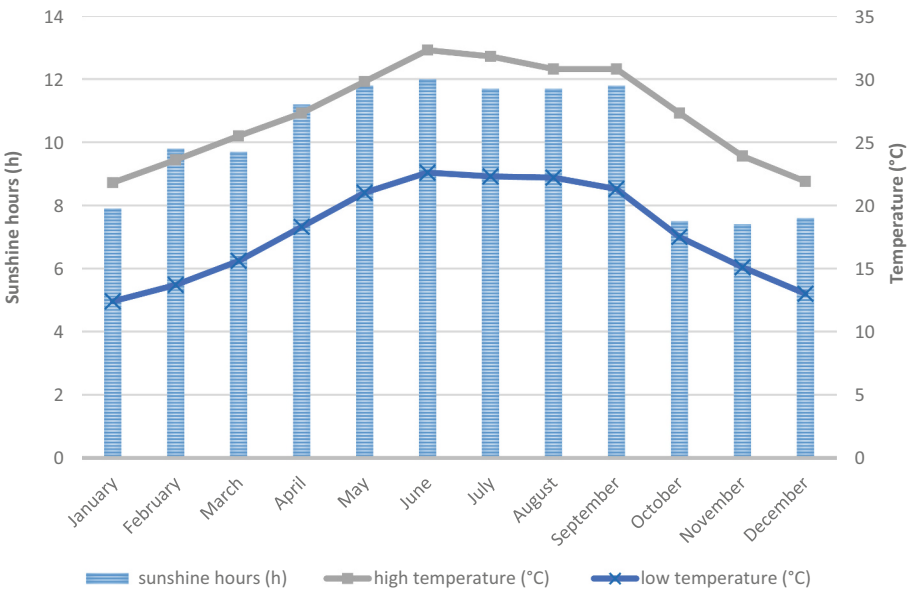

Fig. 3. Average Sunshine and Monthly Low and High Temperatures in Abha, Saudi Arabia

Due to the above, as seen in Fig. 3, we have addressed the scenario of the most challenging environmental circumstances, which are the same for the winter solstice day.

It is suggested that the TIM-PS perpendicular construction suppresses the phenomena of heat transmission from the south glass wall to the surroundings through natural convection. The first objective in analyzing the Trombe wall's performance is determining its thermal efficiency.

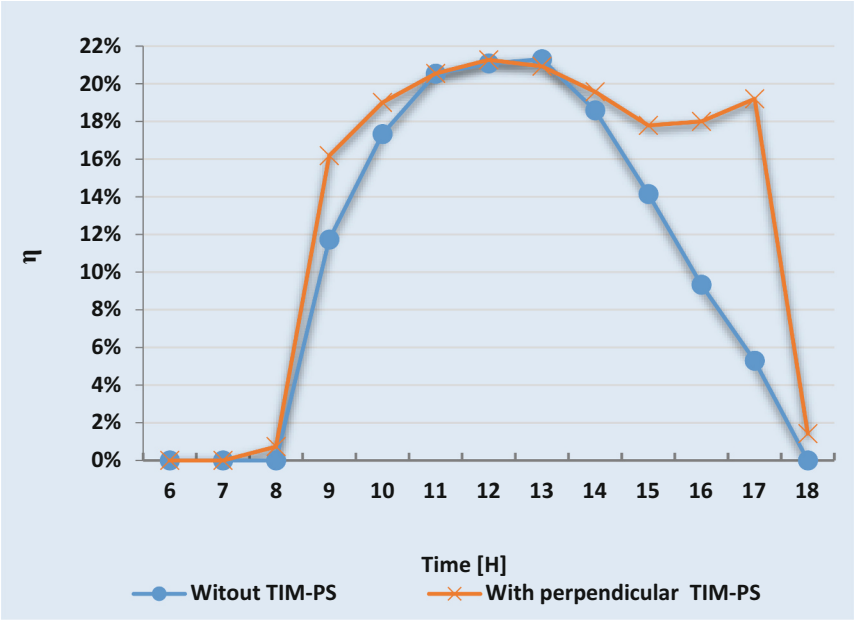

Fig. 4. Conventional Trombe Wall and TIM-PS thermal efficiency

The thermal performance of the Trombe Wall unit is shown in details. Air temperature data for the T-T-W system, with and without ITM-PS, were collected on the basis of temperatures.

These data were then plotted in Fig. 4 at the room inlet and outlet. The air temperatures inside the T-T-W system depend on the outside climate, especially the temperature and the solar radiation. The results demonstrate that solar radiation significantly impacts thermal efficiency and often causes substantial convective heat loss. Integrating TIM-PS into glazing systems greatly amplifies the system's benefits. Convective heat loss between the Trombe wall and the glass south wall can be eliminated by using TIM-PS perpendicularly, increasing thermal efficiency.

It increased from less than 5% to over 19% at 5:00 p.m. Consequently, installed thermal efficiency increases from nine hours for a conventional glass wall to 11 h for a perpendicular glass wall fitted with TIM-PS.

A 2.7 times better performance is achieved by the Trombe TIM-PS wall than by the standard Trombe wall. This efficiency gain is probably due to the reduction of convection losses.

Due to the efficacy of TIM-PS, convection from the Trombe wall to the glazing is impeded, a phenomenon that occurs when the temperature of the wall exceeds that of the glazing (during the most extreme hours of the day). Being efficient is considered linearly proportional to (Tin-Tout) since the heat loss coefficient is proportional to it. Consequently, it has been observed that perpendicular TIM-PS curtail heat dissipation and enhance thermal efficiency.

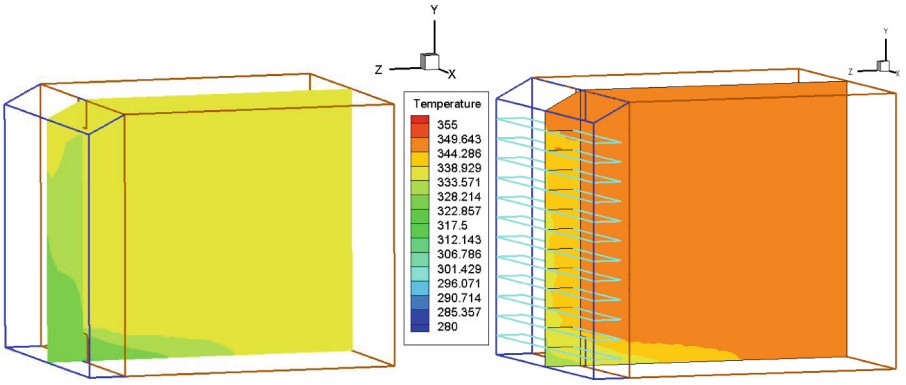

Fig. 5. TIM-PS Trombe Wall and Reference Trombe Wall Temperature Distribution for the Two Configurationon Plan (Yoz)

The interior temperature field in the (yoz) plane, in the Trombe wall and in the adjoining room is compared in Fig. 5, again under conditions with 12 perpendicular TIM-PS and the reference T.W. The temperature distribution for these two cases represents the behavior of the temperature field in the T.W. system at 12:00 p.m., together with the adjacent room. The system's ability to heat the layer of air leaving the room is illustrated by the values obtained, as is its response to the influence of the TIM-PS devices.

The temperature inside the system is not uniform at 12:00 p.m., due to the high level of solar radiation ($I = 780\ W/m^2$). At this time, the radiation is so intense that it generates air movement in the channel by itself. As a result, there were different temperatures at the bottom and top of the air layer. As predicted, the temperature at the top of the air layer, near the entrance to the room, is always higher than that obtained at the bottom of the air layer. Solar radiation is absorbed by the transparent wall; some of this energy is transferred by conduction through the wall, while the rest is transferred to the air in the air space by natural convection. This process produces the distributed temperature pattern. And then, if we pay close attention, we see that the zone with a perpendicular TIM-PS is the one with the highest temperature gradient. In the interstitial space between the south-facing glass wall and the absorber wall, the thermal gradient is vertical, and the temperature oscillates between 335 kelvins and 350 kelvins for a perpendicular TIM-PS configuration. In contrast, for the reference case, the temperature inside the channel

fluctuates between 310 kelvins and 340 kelvins. For the adjacent room, however, it is clear that the T-T-W TIM-PS ensures a more even temperature distribution inside the room.

It is notable that the overall temperature of the T-T-W TIM-PS is significantly higher than that of the reference T-T-W, demonstrating the effectiveness of including the perpendicular TIM-PS in T-T-W optimization, substantially reducing convective heat loss through the south-facing glass wall.

References

1. Alaoui, A.L., et al.: Enhancing energy efficiency for buildings in hot-desert climate: CFD investigation of trombe walls using several thermal fins configuration. Int. J. Thermofluids **22**, 100642 (2024). https://doi.org/10.1016/j.ijft.2024.100642
2. Abdel-Aziz, M.M., Al-Sayad, R., Ibrahim, B.M.: Modelling of the outdoor and indoor parameters affecting the thermal performance of a trombe wall with different spaces. J. Eng. Res. (2023). https://doi.org/10.21608/erjeng.2023.237595.1257
3. Li, R., et al.: Investigation on heat transfer characteristics of multi-duct Trombe wall based on multi-mode heat exchange in winter. Appl. Therm. Eng. **278**, 123311 (2024). https://doi.org/10.1016/j.applthermaleng.2024.123311
4. Bogdanovic, B.V., Randjelovic, J.D., Vasov, S.M., Ignjatovic, G.M., Stevanovic, N.J.: Improving thermal stability and reduction of energy consumption by implementing Trombe wall construction in the process of building design: the Serbia region. Therm. Sci. **22**, 2355–2365 (2018). https://doi.org/10.2298/TSCI180308167B
5. Hernández-Pérez, I., Rodriguez-Ake, A., Sauceda-Carvajal, D., Hernández-López, I., Kumar, B., Zavala-Guillén, I.: Experimental thermal assessment of a trombe wall under a semi-arid mediterranean climate of Mexico. Energies **18**(1), 185 (2025). https://doi.org/10.3390/en18010185
6. Dong, X., Xiao, H., Ma, M.: Thermal performance of a novel Trombe wall enhanced by a solar energy focusing approach. Low-Carbon Mater. Green Const. **2**(1), 8 (2024). https://doi.org/10.1007/s44242-024-00039-5
7. Patel, A.K.: Energy efficient building design with solar passive heating and ventilation systems. Glob. J. Eng. Technol. Adv. (2024).https://doi.org/10.30574/gjeta.2024.20.2.0144

Circular Economy

Valorization of Office Paper Recycling Processes

Fatma Zahra Sahraoui(✉), Imen Maatouk, Arwa Turki, and Asma El Ouediani

Laboratory of Textile Engineering "LGTex", University of Monastir, 5070 Ksar-Hellal, Tunisia
fatmazahra.sahraoui@enim.u-monastir.tn

Abstract. This study aimed mainly at recycling office paper waste to develop a new paper by exploiting different defibering methods, including the use of seawater to overcome the lack of tap water resources. The study results of the difference between recycled fibers defibered by seawater and tap water with a 2-sample test did not show significant differences in fiber dimensions. However, the result proves the possibility of replacing tap water with seawater to improve water resource management, in order to save precious water resources and reduce costs. And paves the way for the need to strengthen these papers impacted by recycling and defibering.

Keywords: waste office paper · regenerated fiber · fibers defibrated by sea water "FdM"

1 Introduction

The global consumption of paper and cardboard was more than 414 million tons in 2022 and which is increased by 60 MT consumed in the world from 2009 to 2021 [1] where paper represented 3/4 of the tonnage of waste produced due to the increase in economic and administrative activities that generate a large amount of paper waste in offices. This presents an interesting source of raw material to be recycled thus reducing the environmental impact and promoting a circular economy. While, traditional paper recycling has limitations, including washing and chemical treatments require excessive water consumption, 130L for the manufacture of 500 sheets, compared to 51.1L for the production of the same quantity of sheets from wood [2]. As well, the quality of recycled papers is often lower, due to their low strength, caused by the fibers cut into small pieces resulting in shortened fibers which do not make it possible to obtain a high-quality paper product. Lipkiewicz has observed a method to protect the quality of fibers and resulting papers by cutting the paper into pieces with a surface area greater than 25 mm2 during the shredding process does not significantly affect the tensile properties of papers made from recycled fibers [3]. And for an eco-responsible approach aimed at minimizing the use of fresh water while sea water could pose additional challenges, notably in terms of its salinity, sea water contains 96.5% water and of 3.5% salt [4] These salts can affect the structure and strength of fibers, which could influence the quality of recycled paper as well as the sodium chloride content can form hydrochloric acid with cellulose which causes damage to the fibers [7]. On the other hand, sea salt is used in the paper industry

N. Meksi et al. (Eds.): ICACE 2024, SPM 97, pp. 19–25, 2025.
https://doi.org/10.1007/978-981-95-4188-1_3

for the production of bleached pulp. It is used to remove impurities from the pulp and to improve the quality of the paper [8].

This research explores the shredding method approved by Lipkiewicz with the use of seawater in the defibration of waste paper. However, characterization is then introduced, allowing the impact of defibration and shredding on pulp quality to be assessed.

2 Materials and Methods

Materials: For our study, we used waste printed-papers (monochrome ink) collected from LGTex laboratory and sea water from Monastir touristic-area.

Reducing the Size of Office Paper Waste: The A4 paper was cut manually into pieces having a surface area between 25 mm^2 and 40 mm^2 according to the Lipkiewicz method. Then these pieces were soaked in sea-water then tap-water for 12 h, moving on to the grinding of these soaked pieces until total defibration at a pulp concentration of 12%, using a 3500rpm laboratory mixer, and finally the drying of the pulp according to ISO 287.

Measurement of the Dimensions of the Recycled Fibers: Using a Leica DM500 optical microscope with a magnification of 4×0.10 and 10×0.22, the measurement of the length and width of the 300 fibers according to ASTM D5103–07 (2018) was made.

Evaluation: The distribution of the lengths and widths of fibers defibrated by two types of water (sea water, tap water) was examined with the normal distribution curve and the difference between fibers with a 2-sample test, using the "Minitab" software.

3 Results and Discussions

3.1 Impact of Shredding on Recycled Fibers

Figure 1 and Fig. 2 show a microscopic view at different magnifications for both fibers defibrated with sea water "FdM" (see Fig. 1.A and Fig. 2.A) and with tap water "FdR" (see Fig. 1.B and Fig. 2.B).

The microscopic observation (see Fig. 1 and Fig. 2) shows the presence of both intact fibers (green circle) and cut fibers (blue circle). The vast majority of fibers remain intact, this indicates that there is a slight shortening of the length of the FdM and FdR fibers defibrated by the two types of water (sea water, tap water), in accordance with the study results of Lipkiewicz, et al. (2021) which postulates that the method cut into pieces with a surface area between 25 mm2 and 40 mm^2 it does not significantly influence the properties of waste paper pulp.

And to confirm the modification obtained between the structure of fibers defibrated by sea water "FdM" and the fibers defibrated by tap water "FdR" it would be necessary to measure the dimensions of the fibers by examining the distribution of their lengths and widths.

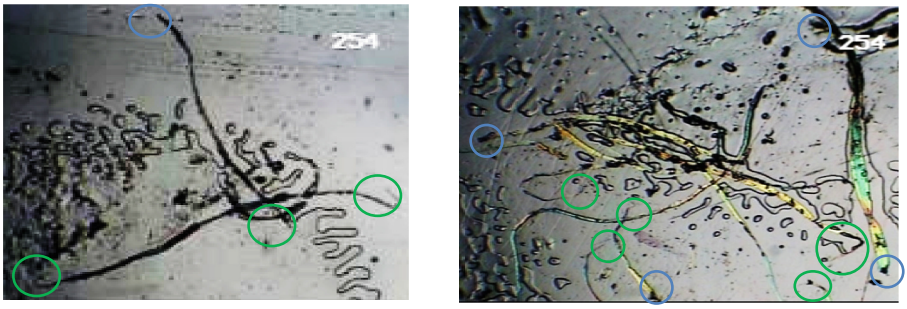

A. FdM **B.** FdR

Fig. 1. Microscopic view of fibers with 4 × 0.10 (A) FdM and (B) FdR

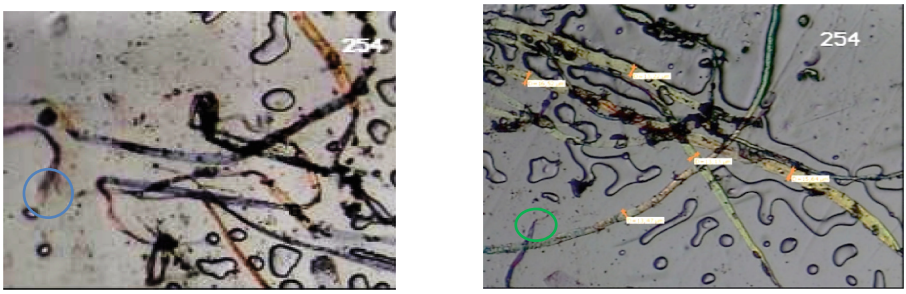

A. FdM **B.** FdR

Fig. 2. Microscopic view of fibers with 10 × 0.22 (A) FdM and (B) FdR

3.2 Evaluation of Recycled Fiber Morphologies

Figure 3 and Fig. 4 show the dispersion of the length and width of both fibers (fibers defibrated by sea water "FdM" in red and fibers defibrated by tap water "FdR" in blue).

The fibers defibrated by tap water "FdR" lengths (the blue histogram (see Fig. 3)), were centered between 0.6 and 1.1 mm and correspond well to the fitted distribution line with a mean of 0.8421 mm. While the lengths of fibers defibrated by sea water "FdM" (the red histogram (see Fig. 3)), were more dispersed between 0.5 to 1.2 mm and they are slightly shifted compared to the fitted distribution with mean of 0.8658 μm Which translates into the fact that the lengths fibers defibrated by tap water are more homogeneous than the lengths fibers defibrated by sea water "FdM". This result can be attributed to the influence of sea salts present in seawater.

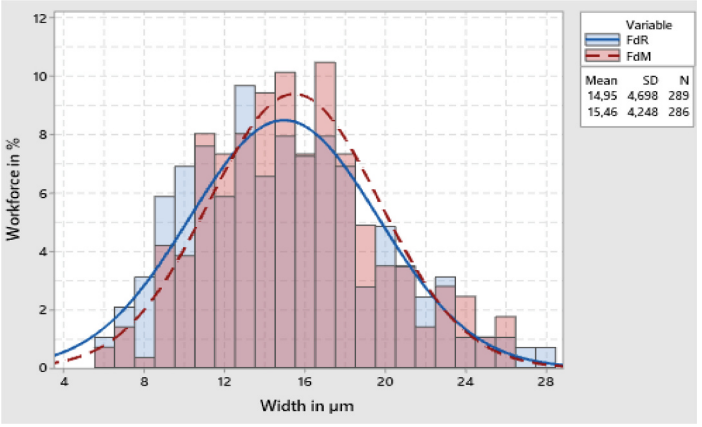

Fig. 3. Recycled fiber length distribution

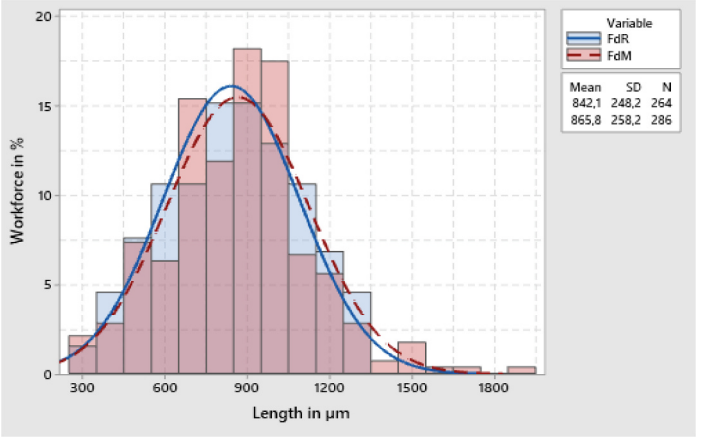

Fig. 4. Recycled fiber width distribution

The widths of fibers defibrated by tap water "FdR" (the blue histogram (see Fig. 4)), were more dispersed from 9 to 18 µm and which move away from the mean of 14.95 µm especially on the side where the fiber is thin with a peak of 13 µm for 9.8%. This indicates that the majority of fibers defibrated by tap water "FdR" lose their swelling capacity. This was also explained by Lyne and Gallay.1950 who concluded that bleached pulps, showed a more marked tendency to lose their swelling capacity during drying, compared to unbleached pulps (see Fig. 6). It is also suggested by Stone and Scallan (1966) as well as Ruvo and Htun (1983) that the loss of swelling capacity is related to the closure of pores in the cell walls [9]. On the other hand, the widths of fibers defibrated by sea water "FdM" (the red histogram (see Fig. 4)), occur at values between 9 and 21 µm with a peak extending from 14 to 17 µm of 10.5% and corresponds well to the adjusted distribution

line of mean of 15.46 µm which indicates that the presence of sea salts causes swelling of the fibers and opening their pores. This leads to say that the presence of ions dissolved in seawater increases the swelling capacity and can cause the rupture of inter-fiber bonds which weaken the properties of the fibers and paper produced thereafter.

Figure 5 and Fig. 6 represent a comparison of the mean lengths in mm and mean widths in µm of the different fibers; virgin fibers (blue), recycled fibers (green) and fibers from our study (orange).

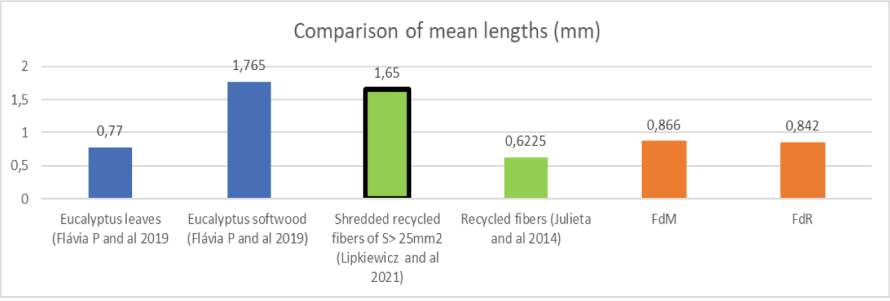

Fig. 5. Histogram of average lengths of different fibers. (Color figure Online)

The quality of regenerated fibers (green) is often inferior compared to virgin fibres (blue). The fibres examined in our study (orange) have length values of 0.8658 mm and 0.8421 mm for fibres defibrated by seawater "FdM" and defibrated by tap water (FdR) respectively. These length results are almost equal and which shows that the use of seawater has no clear influence on fibre length. However, Češek & Milichovský (2005) showed that increasing the degree of mixing of the pulp increases fiber shortening [7]. On the other hand, Fig. 5 shows that the method conducted by Lipkiewicz, and al (2021) minimises the decrease in fiber lengths compared to the length of fibers from conventional recycling approved by Julieta which were equal to 0.6225 mm [8].

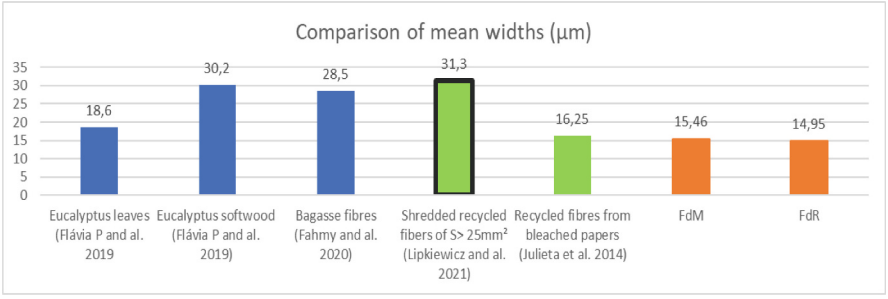

Fig. 6. Histogram of average widths of different fibers. (Color figure Online)

Although the width distribution (Fig. 4) is different but the average values (Fig. 6) of two fibers are almost equal at 15.46 and 14.95 µm for the width of fibers defibrated by

sea water "FdM" and the width of fibers defibrated by tap water "FdR" respectively. This is confirmed by the bleaching effect [8] where the width values of recycled bleached paper fibers range between 15.7 to 16.8 μm with an average of 16.25 μm (Fig. 6).

3.3 Determination of the Statistical Significance of Recycled Fiber Dimensions in Our Study

To comprehend whether the differences in length and width measurements among the two fibers are statistically significant (i.e., FdR ≠ FdM). A 2-sample test with 95% confidence interval CI was used.

Table 1. Estimation of fiber difference.

	Mean length	Mean width
P value	0,273	0,171

In Tab.1, the difference of means in the evaluations of mean fiber length and width, the P value is less than 0.5 for length and width respectively with 0.273 and 0.171, so the null hypothesis where FdR = FdM is verified and there is no significant difference between defibration with seawater and tap water on fiber length and width. This result proves the possibility of replacing tap water with seawater to improve water resource management.

4 Conclusion

In our study, we focused on recycling office paper to create a new product while reducing recycled fiber quality using a specific cutting method and minimizing tap water consumption by substituting it with sea water. We examined how sea water affects the morphological modification of recycled fibers compared to tap water. The evaluated morphological parameters are the length and width of the fibers identified using optical microscope equipment. First, the microscopic view (Fig. 1 and Fig. 2) indicates that most fibers remain intact, suggesting a slight shortening of FdM and FdR fibers treated with sea water and tap water using the approved cutting method. The length distribution (Fig. 3) of fibers defibrated by tap water "FdR" appears normal, while lengths of fibers defibrated by sea water "FdM" are more dispersed. FdR fibers are more homogeneous in length than FdM fibers, which are affected by dissolved sea salts. And for the fiber width distribution (Fig. 4) show that in FdM, sea salts cause fiber swelling and pore opening, unlike the FdR Dissolved seawater ions enhance swelling and can break inter-fiber bonds, weakening the fibers and resulting paper properties. Then a 2-sample test confirmed that there is no significant difference between fiber dimensions from defibering with seawater and tap water. This suggests that seawater can replace tap water in paper recycling, improving water resource management and reducing fresh water waste.

To achieve the best physical-mechanical properties of the final product, we can mix seawater with tap water and reinforce the papers with bio-sourced minerals like calcium carbonate from eggshell waste (ECC).

References

1. Statista: Paper and paperboard: Global apparent consumption (2021). https://fr.statista.com/statistiques/561149/consommation-mondiale-papiers-cartons/. Accessed 21 Nov 2023
2. Papiernetz: Argumente für Recyclingpapier. https://www.papiernetz.de/argumente-fuer-recyclingpapier/. Accessed 21 Nov 2023
3. Lipkiewicz, A., et al.: Impact of shredding degree on papermaking potential of recycled waste. Sci. Rep. **11**(1), 17528 (2021). https://doi.org/10.1038/s41598-021-96325-4
4. Ghaouaci, S.: Cours Licence Aquaculture et Pisciculture – CHIMIE MARINE. Université Hassiba Ben Bouali de Chlef. https://www.univ-chlef.dz/fsnv/wp-content/uploads/Cours-chimie-marine-L3-Aquaculture.pdf. Accessed 21 Nov 2023
5. Pérez, S.: Structure and morphology of cellulose. https://www.researchgate.net/publication/281877184_Structure_et_morphologie_de_la_cellulose. Accessed 11 Nov 2023
6. Tapin-Lingua, S., Meyer, V., Petit-Conil, M.: Biotechnologies dans l'industrie papetière. Techniques de l'Ingénieur. https://www.techniques-ingenieur.fr/base-documentaire/materiaux-th11/papiers-et-cartons-42832210/biotechnologies-dans-l-industrie-papetiere-bio4200/. Accessed 23 Nov 2023
7. Cabalova, L., et al.: The effects of paper recycling and its environmental impact. In: Environmental Management in Practice. IntechOpen (2011). https://doi.org/10.5772/23110
8. Julieta, B., et al.: Office Paper Recyclability: Fibrous Characteristics. https://www.semanticscholar.org/paper/OFFICE-PAPER-RECYCLABILITY%3A-FIBROUS-CHARACTERISTICS-Julieta-Maria/66219e2c3d7c9e246df371bfbc06517dcfc846d0. Accessed 23 Nov 2023
9. Hubbe, M.A., Venditti, R., Rojas, O.J.: What happens to cellulosic fibers during papermaking and recycling? A review. BioResources **2**(4), 739–788 (2007)

Carbon and Water Footprint of Jeans - A Life Cycle Assessment Approach

Mouna Hadj Nasr[1], Hassen Hedfi[2(✉)], and Ayda Baffoun[1]

[1] Textile Materials and Processes Research Unit MPTex, National Engineering School of Monastir, University of Monastir, 5019 Monastir, Tunisia
hadjnasrmouna@gmail.com

[2] Mechanical Engineering Laboratory LGM, National Engineering School of Monastir, University of Monastir, 5019 Monastir, Tunisia
hadjnasrmouna@gmail.com

Abstract. The jeans sector is renowned for its significant environmental footprint due to high consumption of water and energy consumption, along with the application of chemicals throughout various stages of production. Life Cycle Assessment (LCA) is the most widely used method for calculating the environmental impact of products. This study adopts a cradle-to-gate approach to evaluate the environmental impacts of a pair of jeans, focusing on two major impact categories: global warming and water consumption. Results reveal that a single pair of jeans emits 12.6 kg of CO_2 eq, primarily attributable to the fabric manufacturing phase, which accounts for 47% of total emissions. Additionally, water consumption per pair of jeans amounts to 0.606×10^{-3} m^3, with the cotton growing phase responsible for 82% of the total consumption. By identifying key environmental hotspots, this research supports the implementation of targeted actions to minimize damage. These insights support the transition toward a more environmentally friendly textile industry.

Keywords: Life Cycle Assessment · Jeans Sector · Environmental sustainability · SimaPro®

1 Introduction

The clothing industry, one of the largest globally, is widely known for its environmental damage throughout the entire life cycle of a garment [1]. Jeans manufacturing is recognized as one of the most environmentally impactful sectors in the textile industry [2]. The rapid expansion of jeans production is intensifying this environmental impact [3]. Various studies estimate that producing a single pair of jeans requires between 5,700 to 15,000 L of water [2], with other sources citing a range of 9,000 to 11,000 L [3]. Another report indicates a total water consumption of 3,781 L throughout the jeans' entire lifecycle [4]. Regarding climate change impact, a study found that jeans manufacturing generates approximately 96 million tons of CO2 eq annually [2]. Carbon footprint assessments also show that emissions range from 33.4 kg [4] to 90.37 of CO_2

N. Meksi et al. (Eds.): ICACE 2024, SPM 97, pp. 26–31, 2025.
https://doi.org/10.1007/978-981-95-4188-1_4

eq [5] over the lifetime of a pair of jeans. The jeans industry needs to adopt sustainable measures covering the entire product lifecycle to reduce its environmental impact. This requires a comprehensive assessment of each stage in the supply chain, from raw material extraction to jeans disposal. Life Cycle Assessment (LCA) is designed to ensure product sustainability and support environmental decision-making [3]. This study analyzes the life cycle of a single pair of jeans, chosen as a benchmark given their widespread popularity - jeans are worn by nearly half of the world's population [6].

Few LCA studies cover jeans specifically [2, 4, 7–10]. This research aims to address this gap by integrating robust and recent (2024) primary data from a Tunisian manufacturer for jeans manufacturing processes, including cutting, sewing, washing, and finishing. More specifically, this study aims to analyze the carbon and water footprints of a pair of jeans while identifying the main factors contributing to these impacts.

This study is structured as follows: Sect. 2 covers methodology, detailing the research scope and the data collection process. Section 3 provides life cycle impact assessment (LCIA) results, focusing on carbon and water footprints and discussing the primary impact sources. Finally, Sect. 4 presents the conclusions.

2 Material and Methods

For this study, we employed the LCA approach in compliance with ISO 14040 and ISO 14044 standards [11, 12]. LCA is a systematic method for assessing the environmental impacts of a product throughout its lifespan, involving four key stages: Goal and scope definition, Life Cycle Inventory (LCI), life cycle impact assessment (LCIA), and interpretation [13].

2.1 Goal and Scope

The primary goal of this LCA study was to assess the carbon and water footprints of a single pair of jeans. The chosen functional unit is "the production of men's size 32/32 jeans that weighs 0.6 kg". This analysis is conducted within the "cradle-to-gate" system boundaries (see Fig. 1). Covering raw materials production, denim fabric production, transportation, and the manufacturing processes (i.e. cutting, sewing, washing, and finishing) of the jeans. Therefore, the study excludes the use and end-of-life phases, as well as the production of infrastructure and machinery.

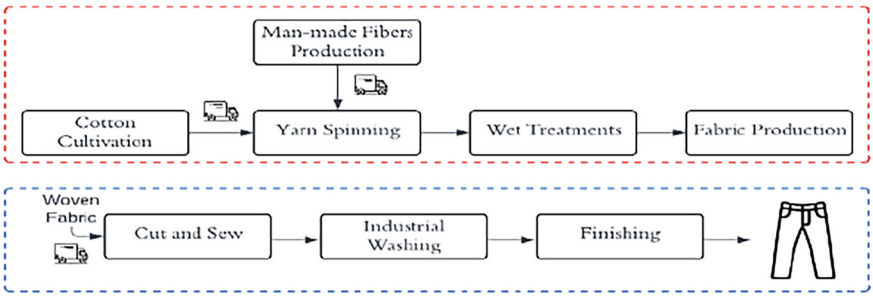

Fig. 1. System boundaries of the analyzed jeans under the cradle-to-gate approach.

2.2 Data Collection

The inventory was developed using primary data, consisting of site-specific information gathered from Tunisian jeans mill in 2024, specifically for the processes within the blue-outlined study boundaries. When primary data were unavailable, secondary data were sourced from the Ecoinvent (v.9.3.1) database and previous reports (for processes within the red-outlined boundaries). Therefore, data for stages such as raw materials and denim fabric production are mainly based on hypothetical scenarios and assumptions. It is also essential to note that transport between various stages has been considered, except when processes occur within the same facility or when facilities are close to each other. A summary of the data used in this study is provided in Table 1.

Table 1. Data sources.

Data	Source	Notes
Cotton cultivation and ginning	Ecoinvent (v.9.3.1)	Data based on Cotton Inc. (2016)
Man-made fibers production	[8]	Country specific, China
Yarn Spinning	[8]	We substituted the used Electricity Mix with 'Electricity, low voltage {EG}'
Wet treatments (dyeing and bleaching)	[8]	–
Fabric production	[8]	–
Cut and sew	Site-specific data	Jeans mill based in Tunisia, 2024
Industrial washing	Site-specific data	Jeans mill based in Tunisia, 2024
Finishing	Site-specific data	Jeans mill based in Tunisia, 2024
Ship Transportation	Ecoinvent (v.9.3.1)	Transport, freight, sea, container ship {GLO}
Road Transportation	Ecoinvent (v.9.3.1)	Transport, freight, lorry 16–32 metric ton, EURO3 {RoW}

3 Results and Discussion

3.1 Life Cycle Impact Assessment

The third phase of the LCA, per ISO 14044, is the LCIA. During this phase, the LCI inputs and outputs are assessed to determine their impacts on human health and the environment [2]. This study examined two impact categories: global warming and water consumption, using the ReCiPe 2016 v1.1, midpoint, Hierarchist (H) method in SimaPro® 9.5 software. The priority given to these two impact categories stems from two main considerations. Firstly, to respond to society's growing concern about global warming, which is consistently highlighted in all LCA studies and is the most evaluated impact category.

Furthermore, the substantial use of water in jeans production is particularly critical in the context of Tunisia's persistent water shortage crisis. Table 2 presents the LCA results for producing one pair of jeans (0.6 kg).

Table 2. Characterized LCA results of jeans production.

Impact category	Unit	Value
Global Warming	Kg CO_2 eq	12.6
Water Consumption	m^3	0.606

3.2 Contribution Analysis

A contribution analysis was carried out to pinpoint the primary causes of the environmental impact throughout the jeans' production processes, as shown in Fig. 2. Regarding the global warming indicator, the fabric manufacture phase is responsible for 47% of the total impact. This significant contribution is mainly due to the resource-intensive processes involved, such as spinning, wet treatments (including warp yarn dyeing and weft yarn bleaching), drying and weaving, all of which require substantial electricity and heat. The jeans production phase is the second-largest contributor to global warming, accounting for 38%, primarily due to fossil fuel use for electricity and heating, particularly during industrial washing, drying, cutting, and sewing. Meanwhile, the cotton-growing phase has the lowest global warming impact, accounting for just 15%. This is mainly explained by the energy consumption involved in preparing the soil, harvesting the cotton, and shipping it to the factories [3].

The analysis revealed that water consumption is highest in the cotton-growing phase, responsible for 82% of the impact. This is mainly due to the high-water demand of cotton [3, 14]. Jeans production phase (including cutting, sewing, washing, and finishing) causes a far smaller impact, yet still represents the second largest contributor to water usage, with 12% of the total impact. This result is consistent with expectations, considering the well-known water-intensive process of industrial jeans washing [14, 15]. Despite being water-intensive, fabric manufacturing has the lowest water consumption impact in this study, possibly due to using generic data; site-specific data might yield more accurate results.

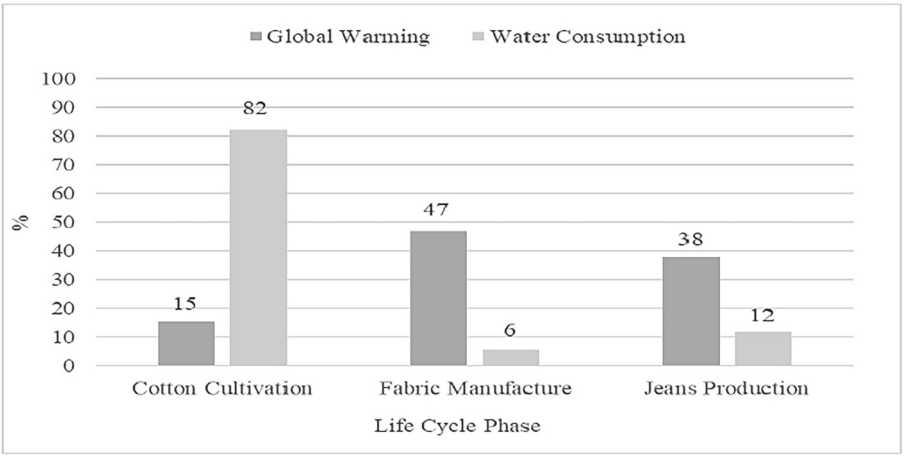

Fig. 2. Contribution of the three life cycle stages: cotton cultivation, fabric manufacture, and jeans production to the environmental impact of jeans.

4 Conclusion

This study examined the carbon and water footprints of a single pair of jeans using a cradle-to-gate approach with recent and reliable data. It highlighted that the fabric manufacturing phase is the primary contributor to global warming impact. The jeans production phase followed closely as the second significant contributor, while the cotton-growing phase had the least impact on global warming. On the other hand, the cotton growing phase is the biggest contributor to water consumption, followed by the jeans production phase and the fabric manufacturing phase. By analyzing these environmental indicators, we gain insight into the jeans industry's ecological footprint at various stages, helping identify critical areas for implementing effective sustainable strategies to reduce environmental impact and drive forward an eco-friendlier jeans industry.

References

1. Nellström, M., Saric, M.: A comparative life cycle assessment of nudie jeans' repair and reuse concept (2019)
2. Åslund Hedman, E.: Comparative life cycle assessment of jeans: a case study performed at nudie jeans (2018)
3. Muthu, S.S.: Sustainability in Denim. Woodhead Publishing, Cambridge (2017). ISBN 9780081020432
4. Levi Strauss & Co. The Life Cycle of a Jean. Understanding the Environmental Impact of a Pair of Levi's ® 501 ® Jeans (2015)
5. Luo, Y., Wu, X., Ding, X.: Carbon and water footprints assessment of cotton jeans using the method based on modularity: a full life cycle perspective. J. Clean. Prod. **332**, 130042 (2021). https://doi.org/10.1016/j.jclepro.2021.130042
6. Athey, S.N., et al.: The widespread environmental footprint of indigo denim microfibers from blue jeans. Environ. Sci. Technol. Lett. **7**, 840–847 (2020)

7. Arvidsson, E.: Environmental Comparison of Jeans Made from Organic Cotton and Conventional Cotton Using LCA A Case Study at J . Lindeberg (2019)
8. Sandin, G., Roos, S., Spak, B., Zamani, B., Peters, G.: Environmental Assessment of Swedish Clothing Consumption – Six Garments, Sustainable Futures (2019)
9. Morita, A.M., Moore, C.C.S., Nogueira, A.R., Kulay, L., Ravagnani, M.A.D.S.S.: Assessment of potential alternatives for improving environmental trouser jeans manufacturing performance in Brazil. J. Clean. Prod. **247**, 11915 (2020). https://doi.org/10.1016/J.JCLEPRO.2019.119156
10. Bongiovanni, R.G., Tuninetti, L.: Análisis Del Ciclo de Vida de Un Jean Producido En Argentina. R. Latino-amer. em Aval. do Ciclo de Vida. **2**(1), 9e34, 9–34 (2018). https://doi.org/10.18225/LALCA.V2I1.3942
11. The International Organization for Standardization ISO 14040:2006, Environmental Management—Life Cycle Assessment—Principles and Framework Available online: https://www.iso.org/obp/ui#iso:std:iso:14040:ed-2:v1:en. Accessed 6 Aug 2024
12. The International Organization for Standardization ISO 14044:2006 - Environmental Management—Life Cycle Assessment—Requirements and Guidelines https://www.iso.org/standard/38498.html. Accessed 6 Aug 2024
13. Şener Fidan, F., Kızılkaya Aydoğan, E., Uzal, N.: An integrated life cycle assessment approach for denim fabric production using recycled cotton fibers and combined heat and power plant. J. Clean. Prod. **287**, 125439 (2020). https://doi.org/10.1016/J.JCLEPRO.2020.125439
14. Zhao, M., et al.: Virtual carbon and water flows embodied in global fashion trade-a case study of denim products. J. Clean. Prod. **303**, 127080 (2021)
15. Sülar, V., Soy, B., Yağci, K.: A case study for water footprint assessment of a denim product. TEXTEH Proc. **2021**, 142–147 (2021). https://doi.org/10.35530/tt.2021.55

Sustainable Textiles

Comparative Analysis of Natural and Synthetic Resins for Eco-Friendly Hydrophobic Treatments in Textile Applications

Wafa Ghedira[1,2(✉)], Marwa Souissi[1,3], Fernando Carrillo Navarrete[4], Chedly Boudokhane[1,5], and Hatem Dhaouadi[1,2]

[1] Laboratory of Research Environmental Chemistry and Clean Processes, Faculty of Sciences of Monastir, University of Monastir, 5019 Monastir, Tunisia
wafa.ghedira@fsm.rnu.tn
[2] Department of Chemistry, Faculty of Sciences of Monastir, Monastir, Tunisia
[3] Higher Institute of Technological Studies (ISET) of Ksar-Hellal, 5070 Ksar-Hellal, Tunisia
[4] Institut d'Investigació Tèxtil I Cooperació Industrial de Terrassa (INTEXTER), Universitat Politècnica de Catalunya, Colom 15, 08222 Terrassa, Spain
[5] Societé CHIMITEX PLUS, 4000 Sousse, Tunisia

Abstract. With growing concerns over the use of hazardous substances in textile waterproofing treatments, this study investigates the potential of natural and synthetic resins as safer alternatives to harmful fluorinated compounds that pose risks to human health. An eco-friendly process was employed to treat cotton fabric using various resin formulations. The chemical compositions of three distinct resins were analyzed using Fourier Transform Infrared Spectroscopy (FTIR). These resins were designed to enhance the hydrophobic properties of the textile, thereby improving water resistance. To assess the effectiveness and durability of the treatments, static contact angle measurements were performed, with results exceeding 100°, indicating good water repellency. In addition, mechanical properties, morphological analyses and color fastness evaluation, including wash, crock, and light fastness, confirmed that the treatment provided good durability and stability over time. The findings suggest that the treated fabrics, exhibiting both water repellency and durability, have strong potential for diverse applications in textile product manufacturing.

Keywords: Natural Resin · Synthetic Resins · Contact angle · hydrophobic surfaces · eco-friendly treatment

1 Introduction

In recent years, increasing environmental awareness and stricter regulations have encouraged the textile industry to reduce or eliminate the use of harmful chemicals in waterproofing treatments. Fluorinated resins, which have been widely used for their excellent water-repellent properties, are now being questioned due to their negative effects on human health and the environment. These substances, known as perfluorinated compounds (PFCs), are highly resistant to degradation and have been linked to endocrine disruption, carcinogenicity, and long-term ecological harm [1].

N. Meksi et al. (Eds.): ICACE 2024, SPM 97, pp. 35–42, 2025.
https://doi.org/10.1007/978-981-95-4188-1_5

Studies have shown that PFCs can migrate from treated textiles into the environment, leading to soil and water contamination. This pollution affects aquatic life and can eventually enter the human food chain, raising serious health concerns [2–4]. In response to these risks, the textile industry is now focusing on safer and more sustainable alternatives. These new solutions aim to maintain the water-repellent properties of treated fabrics while protecting both human health and the environment [5–7].

This research aims to address these pressing challenges by developing safer, eco-friendly waterproofing solutions for textile materials [8, 9]. Specifically, the study focuses on replacing fluorinated compounds with non-toxic, sustainable resins that offer comparable performance in terms of water repellency [10]. Recent advancements in bio-based and natural resins have shown promise in providing effective waterproofing without the harmful side effects associated with traditional fluorinated treatments [11]. To achieve this, an innovative and environmentally conscious finishing process will be applied to cotton fabric, utilizing the benefits of alternative resins to deliver effective waterproofing while ensuring safety and sustainability. This approach follows the principles of green chemistry and helps develop sustainable practices in the textile industry.

2 Material and Methods

2.1 Analysis of Resins

The resins employed in the cotton treatment were analyzed using Fourier Transform Infrared (FTIR) spectroscopy with a PerkinElmer spectrophotometer. The spectral range covers from 400 to 4000 cm^{-1}, and the analysis was conducted under conditions of 16 scans at a resolution of 4 cm^{-1}.

2.2 Preparation and Application of Resins Solutions on Textile Supports

The study examined a range of resin compositions: 100% natural resin, Foil T, and PU38, applied individually; combinations of two resins, including 50% natural resin with 50% Foil T and 50% natural resin with 50% PU38; and a three-resin blend consisting of 50% natural resin, 25% Foil T, and 25% PU38. These resins were suspended in a solution of alcohol and water, using a dispersing agent to ensure proper distribution. One liter of this suspension was prepared for immersion of the fabric mixture, which was then processed to remove excess liquid by passing it through the rollers of a padding machine. The impregnated fabric samples were dried at room temperature in a laboratory dryer (Rame ERNST BENZ AG textile machines, Rümlang-Zurich) and subsequently heat-treated to promote polymerization.

2.3 Characterizations of Treated Cotton

2.3.1 Contact Angle Measurement

Contact angle measurements were conducted using the sessile drop method with a DSA 100 drop shape analysis instrument (Krüss GmbH, Hamburg). The contact angle (θ) is

calculated using the equation:

$$\theta = 2 \times \text{Arctg}\frac{2 \times h}{D} \quad (1)$$

Samples were secured on a measurement table, and a droplet of distilled water was placed on their surface, illuminated with an optical illuminator. A stereo microscope captured an image of the droplet, and three points corresponding to the droplet's extremities and apex were selected using a computer mouse. The surface is classified as hydrophilic if the contact angle is less than 90° and hydrophobic if it exceeds 90°[12].

2.3.2 Mechanical Properties

The tensile strength and elongation at break of the samples were measured using tensile testing machine type Zwick, Germany, in accordance with ISO 13934-1. Tests were conducted with a gauge length of 50 mm and a crosshead speed of 100 mm/min. The reported results represent the average of five measurements per sample.

2.3.3 Morphological Analysis by SEM

The samples were characterized and analyzed using a Phenom scanning electron microscope (Phenom ProX Desktop SEM, Thermo Fisher Scientific, U.S.) to examine the morphology of the cotton fabric treated with various resins.

2.3.4 Durability of the Treatment

To assess the durability of the treated fabric with three mixture resins, standardized tests were conducted. Wash fastness, crock fastness, and light fastness were evaluated in accordance with ISO 105-C06, ISO 105-X12, and ISO 105-B02 standards, respectively.

3 Results and Discussions

3.1 FTIR Analysis

The analysis of the IR spectra provides significant insights into the chemical composition of the three resins utilized in this study. Figure 1, attributed to the natural resin, reveals three strong peaks corresponding to the hydrocarbon C-H bands at 2975, 2920, and 2850 cm^{-1}. Additional bands observed at approximately 730 cm^{-1} and 1465 cm^{-1} correspond to the bending vibrations of C-H in hydrocarbons. Furthermore, bands around 1730 cm^{-1} are indicative of the bending vibrations of C = O in esters and free fatty acids, while bands at approximately 1240 cm^{-1} are associated with the bending vibrations of C-O in esters. Collectively, these FTIR findings substantiate the chemical composition of the natural resin. Figure 2 and 3 present the FTIR spectra of the synthetic resins Foil T and PU 38, respectively. Both spectra exhibit a strong peak in the range of 3300–3500 cm^{-1}, attributed to the N-H band of amides, along with C = O absorption bands of urethane at 1700–1730 cm^{-1} and C-O bands of ether in the range of 1000–1250 cm^{-1}. Together, these FTIR findings confirm the chemical composition of the two synthetic resins based on polyurethane.

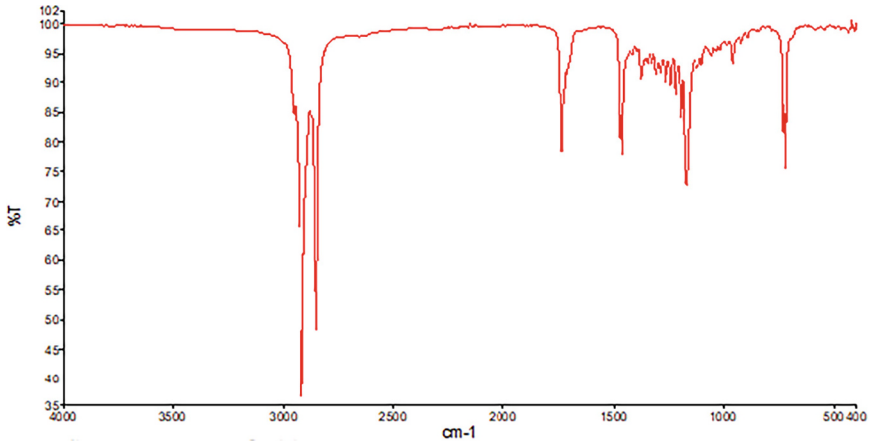

Fig. 1. FTIR spectrum of natural resin

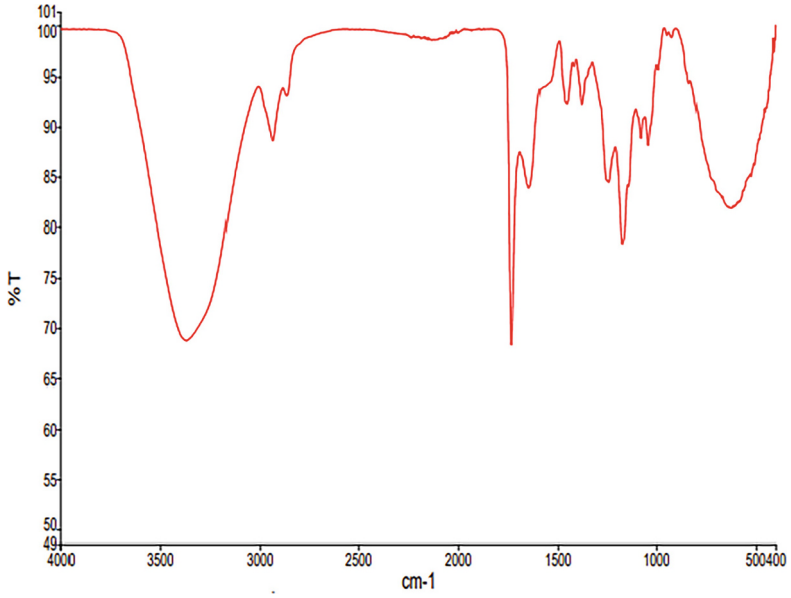

Fig. 2. FTIR spectrum of Foil T

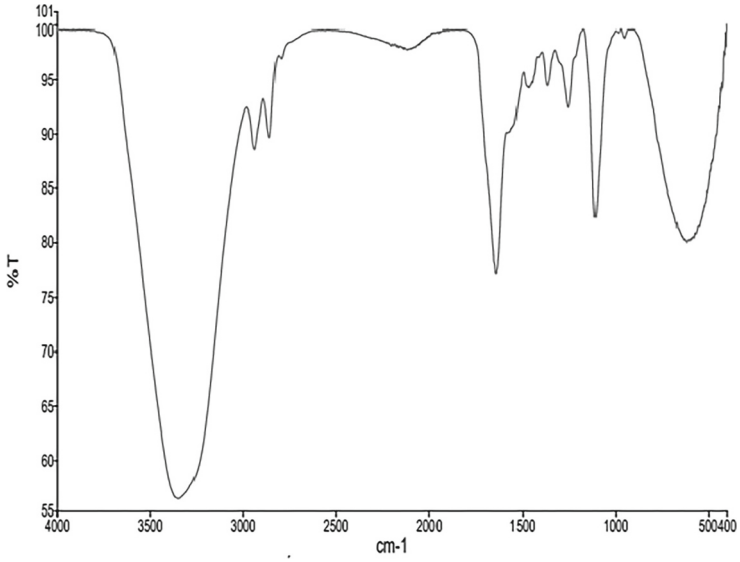

Fig. 3. FTIR spectrum of PU38

3.2 Contact Angle of Coating Process

The contact angle measurements reveal varying degrees of hydrophobicity across the resin compositions studied. As shown on Table 1, the 100% natural resin exhibited a contact angle of 90.8°, indicating significant water repellency. In contrast, both 100% Foil T and 100% PU38 demonstrated complete hydrophilicity with a contact angle of 0°. The mixture of 50% natural resin and 50% PU38 achieved a moderate contact angle of 71°, while the combination of 50% natural resin and 50% Foil T showed a much higher angle of 95.2°, reflecting enhanced water resistance. Notably, the mixture of 50% natural resin, 25% Foil T, and 25% PU38 exhibited the highest contact angle of 105.5°, indicating excellent hydrophobic properties and making it particularly suitable for various applications.

Table 1. Contact angle measurement

Treated samples	Contact angle (°)
100% Natural Resin	90.8
100% Foil T	0
100% PU38	0
50% Natural Resin / 50% PU38	71.0
50% Natural Resin / 50% Foil T	95.2
50% Natural Resin / 25% Foil T/25%PU38	105.5

3.3 Mechanical Properties

The tensile strength and elongation results in table 2 reveal distinct effects of different treatments on cotton fabric. Untreated cotton exhibits the highest tensile strength (1448.74 N) and the lowest elasticity (13.96%). Treatments with natural resin and PU38 lead to noticeable reductions in tensile strength, with a decrease of up to 20.6%, yet significantly enhance the fabric's elongation at break, indicating improved elasticity. Among these, natural resin treatment alone reduces tensile strength the most (1231.18 N), but increases elongation to 19.48%.Combination treatments, such as natural resin with Foil T or PU38, further reduce tensile strength, indicating that multiple treatments may lead to cumulative weakening of the fabric. However, these combinations still improve elongation, highlighting the possibility of tailoring treatments to achieve a balance between strength and flexibility based on the specific performance requirements of the fabric.

Table 2. Tensile strength (Fmax) and elongation at break (εbr) of cotton before and after treatment.

Samples	F_{max} (N)	ε_{br} (%)
Untreated cotton	1448.74	13.96
Treated cotton with natural resin	1231.18	19.48
Treated cotton with Foil T	1340.40	17.27
Treated cotton with PU38	1373.53	19.00
Treated cotton with Natural Resin / PU38	1150.19	18.83
Treated cotton with Natural Resin /Foil T	1135.71	18.43
Treated cotton with Natural Resin /Foil T/PU38	1156.25	17.47

3.4 Morphological Analysis

All SEM images reveal the morphological structure of cotton fiber surfaces following modification with the mixture of three resins (Fig. 4). Compared to untreated cotton (Fig. 5), notable differences are observed, indicating that the coating process has altered the morphological structure of the cotton fibers. This change suggests that the application of natural resin and polyurethane-based resin effectively modifies the surface characteristics of the cotton, potentially enhancing its hydrophobic properties and overall performance. The slight differences observed before and after treatment may be attributed to the deposition of the resin, which creates a protective layer over the fibers, thereby influencing their structural integrity and interaction with moisture.

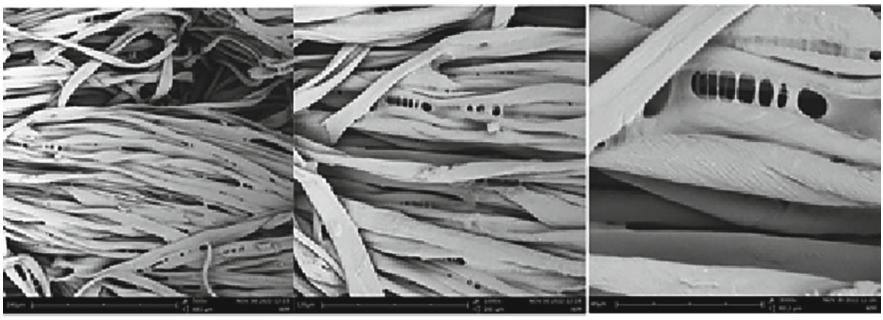

(a) (b) (c)

Fig. 4. Scanning electron microscope (SEM) images of cotton fibers after modification with mixture resins; (a)-magnification 445×; (b)- magnification 1000×; (c)-magnification 2000×.

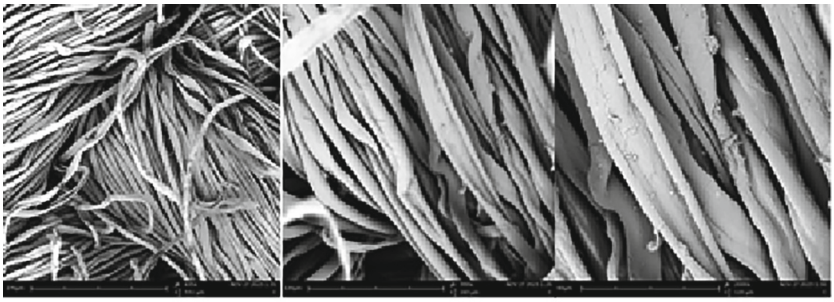

(a) (b) (c)

Fig. 5. Scanning electron microscope (SEM) images of cotton fibers before modification with mixture resins; (a)-magnification 450×; (b)- magnification 1000×; (c)-magnification 2000×.

3.5 Durability of the Coating Process

The durability of the cotton fabric treated with the three resin mixtures was evaluated through standardized tests. The fabric exhibited excellent wash fastness, crock fastness (rating of 5 in both wet and dry conditions), and light fastness (rating of 7-8), demonstrating strong resistance to color change and fading. After 10 washing cycles, the contact angle decreased slightly from 105.5° to 98.0°, confirming a gradual reduction in hydrophobicity while maintaining effective water repellency. These results highlight the treatment's ability to preserve both functional and aesthetic properties over time, making it well-suited for applications such as outdoor textiles and protective clothing.

4 Conclusion

The study's results demonstrate that the cotton fabric treated with resin mixtures exhibited exceptional water repellency, as evidenced by a remarkable contact angle exceeding 100°. Moreover, the treatment displayed excellent durability, retaining its performance

after repeated washing cycles as well as exposure to crocking and light. This elevated contact angle confirms the effectiveness of the eco-friendly treatment and highlights the superior hydrophobic properties conferred to the textile. Such properties significantly enhance the fabric's ability to repel water, making it particularly suitable for a variety of applications that require reliable moisture resistance, including outdoor apparel, protective clothing, and textile products designed for environments where water exposure is a concern. The treatment's effectiveness in creating a robust moisture barrier underscores its potential for commercial viability and practical use.

References

1. Chambers, W.S., Hopkins, J.G., Richards, S.M.: A review of per-and polyfluorinated alkyl substance impairment of reproduction. Front. Toxicol. **3**, 732436 (2021)
2. Glüge, J., et al.: An overview of the uses of per-and polyfluoroalkyl substances (PFAS). Environ. Sci. Process. Impacts **22**(12), 2345–2373 (2020)
3. Brennan, N.M., et al.: Trends in the regulation of per-and polyfluoroalkyl substances (PFAS): a scoping review. Int. J. Environ. Res. Public Health **18**(20), 10900 (2021)
4. Slade, G.D.: Derivation and validation of a short-form oral health impact profile. Commun. Dent. Oral Epidemiol. **25**(4), 284–290 (1997)
5. Zahid, M., et al.: Environmentally benign non-wettable textile treatments: a review of recent state-of-the-art. Adv. Coll. Interface. Sci. **270**, 216–250 (2019)
6. Bashari, A., Koohestani, A.H.S., Salamatipour, N.: Eco-friendly dual-functional textiles: green water-repellent & anti-bacterial. Fibers Polym. **21**, 317–323 (2020)
7. Chaireh, S., Ngasatool, P., Kaewtatip, K.: Novel composite foam made from starch and water hyacinth with beeswax coating for food packaging applications. Int. J. Biol. Macromol. **165**, 1382–1391 (2020)
8. Tawiah, B., Badoe, W., Fu, S.: Advances in the development of antimicrobial agents for textiles: the quest for natural products. Rev. Fibres Textiles Eastern Europe (2016)
9. Singh, A., et al.: Hydrophobicity of cotton fabric treated with plant extract, TiO2 nanoparticles and beeswax. Mater. Today: Proc. **80**, 1530–1533 (2023)
10. Periyasamy, A.P.: Microfiber emissions from functionalized textiles: potential threat for human health and environmental risks. Toxics **11**(5), 406 (2023)
11. Szulc, J., et al.: Beeswax-modified textiles: method of preparation and assessment of antimicrobial properties. Polymers **12**(2), 344 (2020)
12. Ponomar, M., et al.: Sessile drop method: Critical analysis and optimization for measuring the contact angle of an ion-exchange membrane surface. Membranes **12**(8), 765 (2022)

Development of Bio-Functional Textiles Based on Colocynth Oil Microcapsules

Abir Maatallah Nour[1(✉)], Fadhel Jaafar[2], and Néji Ladhari[1,2]

[1] Higher Institute of Fashion, Textile Engineering, Monastir, Tunisia
[2] Springer Heidelberg, Tiergartenstr. 17, 69121 Heidelberg, Germany

Abstract. This study focuses on the development of microcapsules containing colocynth oil, a natural antimicrobial agent. The microcapsules were fabricated using ethylcellulose as a polymer and sodium lauryl sulfate as a surfactant. The encapsulation efficiency reached 92.16%, indicating successful encapsulation of the oil. Morphological analysis revealed a spherical shape with a size distribution that influences the release kinetics of the active ingredient. The microcapsules were characterized for particle size, zeta potential, and thermal properties. The results suggest that the microcapsules are suitable for incorporation into textiles, offering a promising approach for the development of antimicrobial wound dressings and other medical applications.

Keywords: Colocynth oil · Microencapsulation · Biotextile · Antibacterial dressings · Bio compatibility

1 Introduction

Recent advances in medical textiles have led to increasing interest in the use of innovative materials in the manufacture of wound dressings and medical articles [1]. Wound dressings are crucial elements in the management of wounds, whether surgical, traumatic or chronic, as they provide a protective barrier while promoting an environment conducive to healing. Textiles used in the design of wound dressings must meet strict standards in terms of safety, biocompatibility, sterility and functionality in order to ensure optimal therapeutic results [2]. The properties of textiles intended for wound dressings, whether woven, knitted or non-woven, play an important role in their clinical efficacy. They must be designed with materials that guarantee the absence of toxicity, allergic reactions, as well as sterility and biocompatibility [3]. In addition, they must have good mechanical properties to ensure easy handling and adequate wound protection. Sterility is of paramount importance for dressings, requiring that the polymers used in their manufacture can withstand specific physical and chemical conditions.

The essential oil "colocynth", is particularly notable in Tunisia for its medicinal properties, including anti-inflammatory, antidiabetic, antibacterial and antifungal, antioxidant. In addition to its health benefits, it offers interesting prospects for the manufacture of antimicrobial textiles thanks to its antibacterial properties. Its traditional use in

N. Meksi et al. (Eds.): ICACE 2024, SPM 97, pp. 43–48, 2025.
https://doi.org/10.1007/978-981-95-4188-1_6

Tunisian medicine and its local availability promote the development of innovative textiles while supporting sustainable production practices [4]. In this study, we are focused on the development of microcapsules containing colocynth oil, a natural antimicrobial agent [5].

1.1 Material and Methods

Please note that the first paragraph of a section or subsection is not indented. The first paragraphs that follows a table, figure, equation etc. does not have an indent, either.

Subsequent paragraphs, however, are indented.

Raw Materials: Sodium lauryl sulfate as surfactant, ethylcellulose as polymer, ethyl acetate and cyclohexane as solvents (provided by Philadelphia, United Kingdom and France respectively), and colocynth essential oil (obtained from ALVIA parapharmacy). Preparation of microcapsules: Colocynth oil microcapsules were prepared by dissolving ethylcellulose in ethyl acetate and forming an emulsion with sodium lauryl sulfate in water. The emulsion was poured into water to form the microcapsules, then separated by centrifugation, filtered, and dried [6].

Characterization

- Particle size and zeta potential: measured with a MALVERN ZETASIZER.
- Percentage of encapsulated oil: determined by dissolving the microcapsules in cyclohexane.
- Encapsulation efficiency: calculated by relating the mass of encapsulated oil to the total mass of oil used.
- Morphological analysis: by ThermoFisher Scientific SEM.
- FTIR-ATR spectroscopy: to identify functional groups.
- DSC calorimetry: to analyze the thermal properties of the microcapsules.

2 Results and Discussions

2.1 Quantitative Analysis of the Presence of Colocynth Oil in Microcapsules

Table 1. Mass of oil contained in microcapsules

	Average	CV(%)
Initial mass of microcapsules (mg)	200,11	0,06
Mass of dissolved ethylcellulose (mg)	70,11	6,65
Mass of oil obtained (mg)	129,1	3,31
Percentage of oil (%)	64,96	3,59

Measurements of the amount of colocynth oil encapsulated in ethylcellulose microcapsules were carried out to confirm the presence and percentage of encapsulated oil.

The results, summarized in Table 1, show an average mass of oil obtained of 129.1 mg, representing 64.96% of the mass of the microcapsules. The low standard deviation indicates good reproducibility of the process. Thus, the high percentage of encapsulated oil (65%) suggests that the microcapsules obtained are of the "reservoir" type.

2.2 Encapsulation Efficiency

The encapsulation efficiency, calculated by subtracting the amount of unencapsulated oil from the initial amount of oil used, is 92.16%. This indicates efficient encapsulation of colocynth oil by ethylcellulose.

2.3 Morphological Analysis by Scanning Electron Microscopy (SEM)

Observation of the microcapsules under a scanning electron microscope reveals a generally spherical shape with asignificant dispersion of sizes (see Fig. 1 and Fig. 2). This size variation impacts the kinetics of release of the active ingredient, with larger microcapsules tending to release colocynth oil more slowly compared to smaller ones.

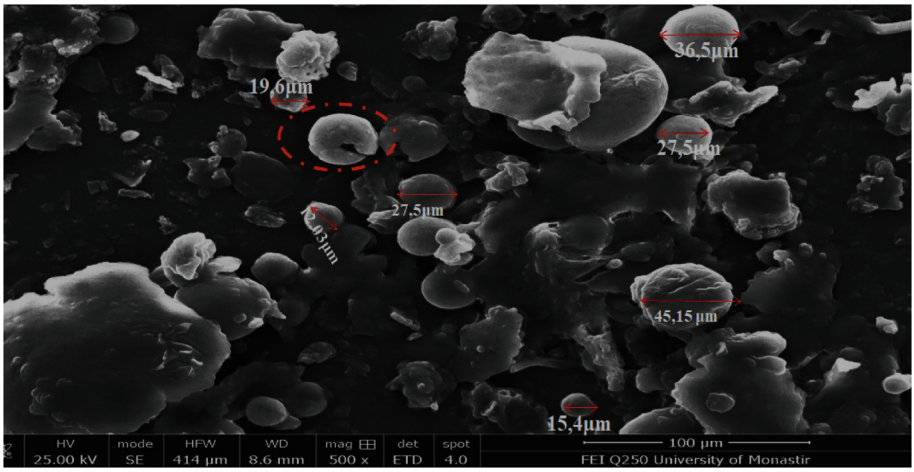

Fig. 1. Microcapsules containing "colocynth" oil (500× oil (500× magnification, 25 kV, ETD)

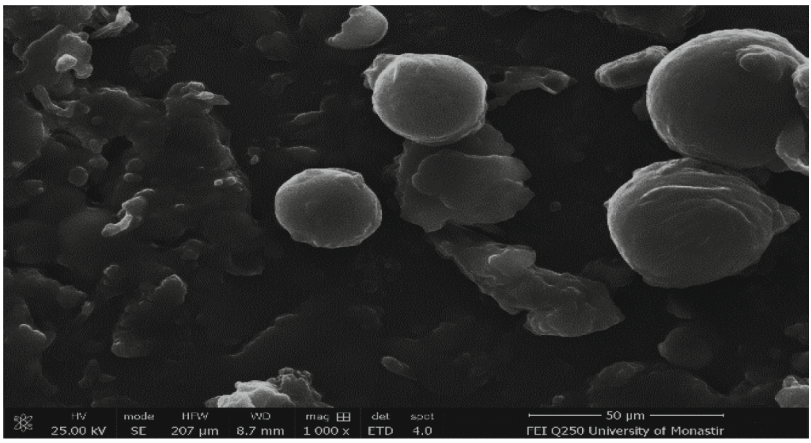

Fig. 2. Microcapsules containing "colocynth" oil (1000× magnification, 25k V, ETD)

2.4 Granulometric Analysis by Laser Granulometer (MALVERN "ZETASIZER" NANO SERIES

A notable observation from the analysis of these data is that as successive dilutions are made, the microcapsules display specific characteristics, they become smaller and more evenly distributed in terms of size. This trend is accompanied by a decrease in the Poly Dispersity Index (PDI), indicating a more uniform distribution of particle sizes in the samples. These changes are observed over several successive dilutions (Table 2).

Table 2. Measuring the distribution of the microcapsules obtained

	Dh(nm)	PDI
Sample 1	173,17 ± 4,7 9	0,147 ± 0,01
Sample 2	181,6 ± 4,79	0,144 ± 0,01
Sample 3	186,3 ± 4,79	0,133 ± 0,01

2.5 Fourier Transform Infrared Analysis (FTIR-ATR)

The FTIR-ATR spectrum of the microcapsules shows the presence of characteristic bands of ethylcellulose and colocynth oil (see Fig. 3). The observed vibrations indicate a conservation of the molecular characteristics of ethylcellulose and an interaction with colocynth oil, with specific bands associated with functional groups and characteristic bonds.

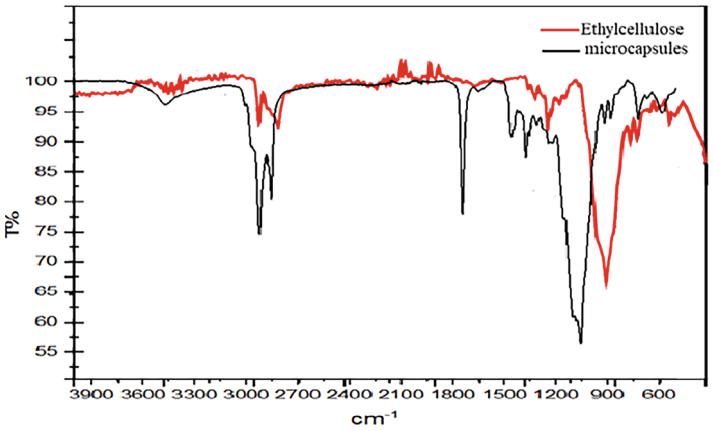

Fig. 3. Fourier transform infrared spectra (FTIR-ATR) of ethylcellulose [7] and (FTIR-ATR) of colocynth oil

2.6 Differential Scanning Calorimetry (DSC) Analysis

DSC thermograms of microcapsules show endothermic and exothermic peaks at different temperatures (See Fig. 4). The results indicate complex thermal reactions and a stabilization phase of microcapsules, with potential degradation of the active ingredient at high temperatures, which is relevant for the stability of microcapsules.

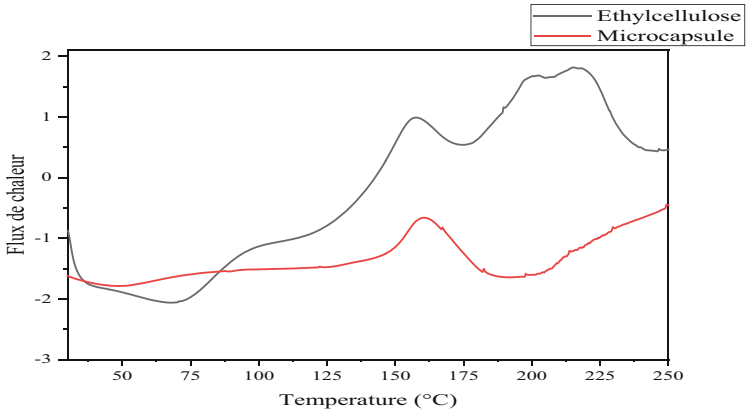

Fig. 4. DSC thermograms of microcapsules and ethylcellulose at a heating rate of 10 °C/min

3 Conclusion

This study successfully developed microcapsules containing colocynth oil, a natural antimicrobial agent with potential applications in textile-based wound dressings. The microencapsulation process demonstrated high efficiency, resulting in a significant amount of encapsulated oil. The microcapsules exhibited a spherical morphology and a size distribution that can influence the controlled release of the active ingredient.

The characterization of the microcapsules revealed their suitability for incorporation into textile materials. The presence of colocynth oil within the microcapsules offers a promising avenue for the development of antimicrobial textiles with enhanced wound healing properties. The results also show that the microcapsules have a homogeneous particle size distribution and retain the bioactive properties of the essential oil, with a significant percentage of encapsulated oil (65%). These characteristics are essential to ensure a controlled and prolonged release of the active agents, thus increasing the effectiveness of the dressings. Further research is warranted to investigate the release kinetics of colocynth oil from the microcapsules under various conditions and to evaluate their efficacy in inhibiting microbial growth on textile substrates.

References

1. Qin, Y.: An overview of medical textile products. Med. Text. Mater. 13–22 (2016)
2. Horžić, M., Marić, K., Bunoza, D.: The temperature dynamics during the healing processing of a surgical (1995)
3. Mogrovejo, A.: Conception et évaluation d'un pansement à libération de deux principes actifs pour le traitement des plaies chroniques. Diss. Université de Lille (2018)
4. Marzouk, B., et al.: Antibacterial and antifungal activities of several populations of Tunisian Citrullus colocynthis Schrad. immature fruits and seeds. J. de mycologie médicale **20**(3), 179–184. Wound. Biomedizinische Technik **40**(4), 106–109 (2010)
5. Le mode d'action des huiles essentielles sur les bactéries – LABORATOIRE DUMANI. (n.d.). https://laboratoiredumani.fr/le-mode-daction-des-huilesessentielles-sur-les-bacteries/2022
6. Jaâfar, F., et al.: Impregnation of ethylcellulose microcapsules containing jojoba oil ontocompressive knits developed for high burns. Fibers Polym. **13**, 346–351 (2012)
7. Reddy, B.B.K., Nagoji, K.E.V., Sahoo, S.: Preparation and in vitro & in vivo evaluation of cephalexin matrix tablets. Braz. J. Pharm. Sci. **54**(03), e17277 (2018). https://doi.org/10.1590/s2175-97902018000317277

Advanced Modeling and Optimization of Acrylic Fibers Cationization Using Combined Response Surface Methodology (RSM) and Artificial Neural Networks (ANN)

Maha Abdelileh[1(✉)], Manel Ben Ticha[2], Nizar Meksi[1,3], and Hatem Dhaouadi[1]

[1] Faculty of Sciences of Monastir, Research Laboratory of Environmental Chemistry and Clean Processes, University of Monastir, 5000 Monastir, Tunisia
maha.abdelileh@gmail.com

[2] Department of Early Childhood, University College of Turabah, Taif University, P.O. Box 11099, Taif 21944, Saudi Arabia

[3] Department of Textile, National Engineering School of Monastir, University of Monastir, 5000 Monastir, Tunisia

Abstract. In this study, the non-polarity and low affinity of acrylic fibers for indigo carmine were investigated. To achieve satisfactory dyeing quality, a cationic agent was used to treat the acrylic fibers. The effects of key cationization process parameters namely, the percentage of the cationizing agent, cationization temperature, duration, and cationization bath pH on the dyeing performance of acrylic fibers with indigo carmine were evaluated. Dyeing results were assessed by measuring color strength (K/S) and dye bath exhaustion (E%). The acrylic cationization process was modeled and optimized using a combined approach of artificial neural networks (ANN) and response surface methodology (RSM). The ANN model demonstrated a strong correlation between experimental and predicted color strength values. Optimization using RSM revealed that the optimal conditions for cationization were: 90% cationic agent, pH 4, 75 min of cationization time, and a temperature of 90 °C, resulting in the best dyeing quality. Cationization of acrylic fibers has proven to be an effective method for enhancing their affinity for indigo carmine.

Keywords: acrylic fibers · cationization · neural network · response surface methodology

1 Introduction

Acrylic fibers are characterized by their low affinity to most textile dyes, low recovery rate and high glass transition temperature. To improve the dyeing performance of acrylic fibers, a number of research projects have been undertaken. The modification of acrylic via the conversion of certain nitrile groups present in the fiber to amino groups has been explored in order to dye acrylic fibers with natural dyes without solvents and under

N. Meksi et al. (Eds.): ICACE 2024, SPM 97, pp. 49–54, 2025.
https://doi.org/10.1007/978-981-95-4188-1_7

atmospheric pressure. This method makes the fiber more hydrophilic and less crystalline. It also increases the affinity of acrylic for anionic dyes at acidic pH [1, 2]. Pre-treatment of acrylic fibers with a cationic agent to improve dyeability has also been reported [3]. It has been shown that increasing the number of quaternary ammonium groups in acrylic fibers increases the rate of absorption of natural dyes by acrylic.

In recent years, the textile industry has explored the application of artificial neural networks (ANN) combined with response surface methodology (RSM) in various processes, such as dyeing cotton with reactive dyes [4], and extracting natural dyes [5]. ANN is a statistical method conceptually inspired by the function of biological neurons. However, its biological accuracy is now of little relevance, instead its success lies in its ability to model complex and nonlinear relationships effectively. The most commonly used ANN model is the multilayer perceptron (MLP), which delivers strong practical results. MLP is typically trained using the gradient backpropagation algorithm, a method widely employed for solving nonlinear problems.

This study aims to address the challenges associated with dyeing acrylic fibers witthe acid dye indigo carmine. To improve the dyeability of acrylic fabrics, we propose the development of a cationization process. Rewin OS was selected as the cationic agent for modifying the acrylic fibers. Additionally, the impact of various process variables on the pretreatment efficiency was investigated. The dyeing process was then modeled using artificial neural networks (ANN), and response surface methodology (RSM) was employed alongside ANN to determine the optimal experimental conditions.

2 Materials and Methods

2.1 Chemicals and Materials

The chemicals used in this study were of analytical grade: sodium hydroxide (NaOH, CDM, Tunisia) and acetic acid (CH_3COOH, Parachimic, Tunisia). Rewin OS (Bezema AG, Switzerland), an ammonium-based preparation, was employed as the cationic agent. Indigo carmine powder ($C_{16}H_8N_2Na_2S_2O_8$, LOBA Chemie, Germany) was used for dyeing the acrylic fabric.

A 100% acrylic fabric was selected for dyeing, with the following specifications: plain weave, mass per area of 230 g/m^2, warp count of 11 yarns/cm, and weft density of 20 yarns/cm**.**

2.2 Cationization of Acrylic Fabric

The acrylic fabrics were treated with the cationic agent Rewin OS before dyeing with indigo carmine under the following conditions: 90% cationic agent, pH 4.5–5, temperature of 50 °C, and a treatment duration of 60 min. The percentage of the cationic agent was selected based on preliminary studies. This pretreatment was performed in a laboratory dyeing machine (Ahiba, DataColor International, USA). After treatment, the acrylic samples were dried at room temperature.

2.3 Dyeing of Acrylic Fabric

The pretreated acrylic samples were dyed in a dye bath containing 5% indigo carmine at a pH of 7, using a liquor ratio of 1:50. The dyeing process was conducted in a laboratory autoclave (Ahiba, Datacolor International, USA) at 100 °C, with a heating rate of 4 °C/min, for 60 min. After dyeing, the samples were rinsed with cold water and dried at room temperature.

2.4 Color Strength Measurements

After dyeing, the color strength (K/S) of the acrylic samples was measured using a Datacolor Spectraflash 600 + spectrophotometer (USA). The color strength (K/S) in the visible region of the spectrum (400–700 nm) was calculated based on the Kubelka-Munk equation [15]:

$$\frac{K}{S} = \frac{(1-R)^2}{2R} - \frac{(1-\mathrm{R}_0)^2}{2R_0} \tag{1}$$

2.5 Dyeing Bath Exhaustion Measurements

The absorbance of the indigo carmine solution was measured before and after dyeing using a UV-visible spectrophotometer (Shimadzu, Japan) at a wavelength of 620 nm. The dye bath exhaustion (E%) was then calculated using the following equation:

$$E(\%) = \frac{(A_0 - A_r)}{A_0} \times 100 \tag{2}$$

where A_0 and A_r are, respectively, the absorbances of the indigo carmine solution before and after dyeing.

2.6 Structure of the Artificial Neural Network (ANN)

In this study, an optimal neural network with a single hidden layer, 8 hidden neurons, 4 input parameters, and color strength as output parameter was used to model the cationization process. The ANN model was designed using MATLAB with its neural network toolbox, based on experimental data. The network was trained using the backpropagation learning algorithm, specifically the gradient descent method with momentum and an adaptive learning rate (traingdx). The model's performance was evaluated by determining the correlation coefficient (R^2) and the mean square error (MSE).

2.7 Design of Experiments

Response surface methodology (RSM) was applied to determine the optimum conditions for the acrylic cationization process. The selected input parameters are the percentage of cationic agent, pH, cationization temperature, and cationization time and the studied response was the color strength (K/S) of the dyed samples. The response surface was generated by Minitab 14 software. According to this design, a total of 27 experiments were performed.

3 Results and Discussions

3.1 Study of the Effect of the Cationization Process

After several tests, it was observed that acrylic fabric exhibits no affinity for indigo carmine, with dyeing experiments showing very low color yield and minimal dye exhaustion. This outcome can be attributed to the presence of anionic carboxylic groups in the structure of acrylic fibers, which repel the negatively charged dye anions during the dyeing process. To enhance its affinity, the acrylic fabric was treated with Rewin OS cationic agent before dyeing. In this section, the influence of the percentage of the cationic agent, pH, cationization time, and cationization temperature on the evolution of color strength and bath exhaustion is shown in Fig. 1.

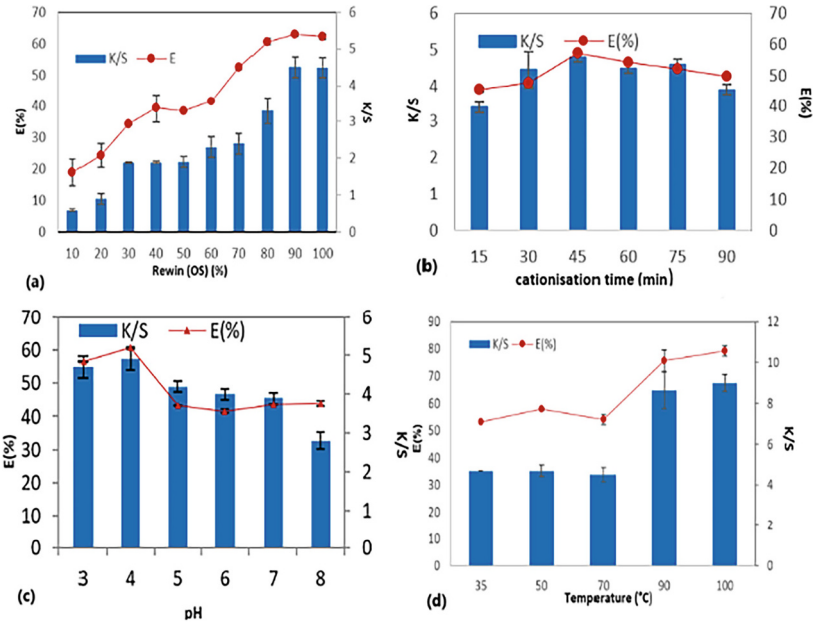

Fig. 1. Evolution of color strength (K/S) and bath exhaustion E(%) as a function of (a): cationizing agent percentage, (b): cationisation time, (c): pH, and (d): cationisation temperature

Figure 1(a) shows an increase in bath exhaustion and color strength as the concentration of the cationizing agent increased from 10% to 90%. This improvement in dyeing performance can be attributed to the growing number of cationic sites in the acrylic fiber with the increasing concentration of the cationizing agent in the bath, which enhanced the fiber's affinity for the anionic dye indigo carmine. Regarding the effect of cationization time, we observe an increase in both color strength and bath exhaustion up to 45 min, likely due to the higher number of cationic sites attracting more dye. Beyond 45 min, both curves plateau, indicating that the fiber has reached saturation with the cationizing agent. Figure 1(c) demonstrates that optimal dyeing quality was achieved

at a pH of 4. Beyond this pH, dyeing parameters progressively declined, confirming that the best dyeing results for acrylic fibers are obtained under acidic conditions. In terms of temperature (Fig. 1(d)), the dyeing parameters remain nearly unchanged up to 70 °C. This can be explained by the inefficiency of the acrylic cationization process at temperatures below the glass transition temperature (Tg) of the polymer. Above 70 °C, a rapid improvement in both dyeing parameters is observed. This enhancement is due to the increased free volume within the polymer chains above Tg, allowing the cationizing agent to penetrate more easily into the fiber.

3.2 Artificial Neural Network (ANN) Modeling of the Acrylic Cationization Process

To develop the neural network, the data were split, with 80% used for training and 20% for testing. During training, all samples were simultaneously processed through the learning algorithm before the weights were updated. The correlation coefficient (R) values for training, validation, testing, and the overall model are presented in Fig. 2. The model's goodness of fit was evaluated using the correlation coefficient, with a result of R = 89%. This indicates that 89% of the sample variation was statistically explained by the model, leaving only 11% of the total variance unexplained.

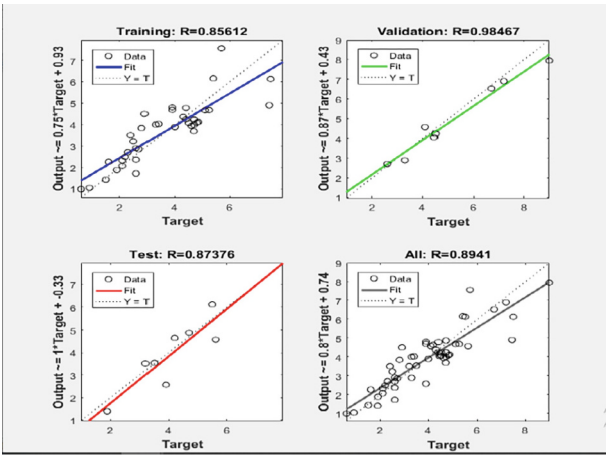

Fig. 2. Regression values for learning, validation, testing, and overall mode

3.3 Optimization of the Acrylic Cationization Process Using the Response Surface Method

The optimization of the cationization process leads to the following optimum conditions: a cationic agent percentage of 90%, a cationization bath pH of 4, a cationization time of 75 min, and a cationization temperature of 90 °C (Table 1). In this case, this table indicates a predicted color strength of 8.06. Dyeing tests were carried out under these optimum conditions. An average color strength of 7.8 was obtained, indicating the validity of these conditions.

Table 1. Optimum conditions for the cationization process

Optimal conditions	Cat (%)	Time (min)	pH	T(C°)	K/S
Values	90	75	4	90	8

4 Conclusion

This research aims to enhance the dyeability of acrylic fabrics dyed with indigo carmine. The application of the cationizing agent Rewin OS to acrylic fabrics before dyeing introduces a novel approach. The influence of different process factors (cationizing agent concentration, pH, cationisation duration, cationisation temperature) on the dyeing quality of acrylic fabric were studied. The ANN model exhibited a good correlation between the experimental and predicted data. Besides, RSM was successfully used to obtain the optimal experimental parameters namely a cationic agent percentage of 90%, a pH of 4, a cationization time of 75 min and a cationization temperature of 90 °C.

References

1. Burkinshaw, S.M., Gotsopoulos, A.: Dyes Pigm. **32**(4), 209–228 (1996)
2. El- Shishtawy, R.M., Ahmed, N.S.E.: ColorationTechnology **121**, 139–146 (2005)
3. Baaka, N., BenTicha, M., Haddar, W., Mhenni, M.F.: J. Renew. Mater. **7**(3), 289–300 (2019)
4. Rosa, J.M., et al.: Clean Technol. Environ. Policy **23**, 2357–2367 (2021)
5. Vedaraman, N., et al.: Chem. Eng. Process. **114**, 46–54 (2017)

Environment

Response Surface Modeling of Amoxicillin Removal from Aqueous Solution: Box–Behnken Experimental Design and Batch Adsorption

Maryi Teieb[1(✉)], Hatem Dhaouadi[1], and Sonia Dridi-Dhaouadi[1,2]

[1] Research Laboratory of Environmental Chemistry and Clean Processes, Faculty of Sciences, Monastir University, Monastir, Tunisia

[2] Preparatory Institute for Engineering Studies, Monastir University, Monastir, Tunisia

Abstract. Water pollution, especially the pollution of surface water resulting from the discharge of industrial and medical waste, has become a significant area of concern in the field of environmental studies. Various methodologies and strategies are utilized for the treatment of these contaminated waters, with the process of adsorption on activated carbon being identified as a promising method for the purification of water. The focus of this research revolves around the exploration of the removal of amoxicillin by employing activated carbon sourced from Prickly Pear Seeds extracted under supercritical carbon dioxide (SC-PPSAC). The response surface methodology was employed to ascertain the optimal conditions for eliminating amoxicillin (AMX) through the utilization of SC-PPSAC. An investigation was conducted on the impact of the experimental factors (initial MB concentration, adsorbent dose, time, and pH) on the adsorption capacity, the optimal parameters included an initial AMX concentration of 140 mg/L, a dosage of 0.1 g of SC-PPSAC, a solution pH of 3, and a time of 120 min. The adsorption kinetics conformed to the model of pseudo-second-order adsorption and demonstrated that the process of adsorption could achieve equilibrium 120-min. The maximum capacity for adsorption of AMX onto our activated carbon calculated to be 17.8 mg/g.

Keywords: Amoxicillin · Adsorption · Response surface · Optimization

1 Introduction

A multitude of harmful substances, such as pharmaceuticals including antibiotics, anti-inflammatory medications, and analgesics, exert adverse effects on organisms and the ecosystem. Even in low levels, these small-scale pollutants can be identified in different reservoirs, including wastewater, surface water, groundwater, and potable water. [1].

The escalation of pharmaceutical contamination in wastewater by minute drug residues has shown a notable increase in recent years, attributed to the surge in cases of influenza and the utilization of pharmaceutical additives. Amoxicillin, belonging to the aminopenicillin family as a β-lactam bactericide, is extensively used for treating bacterial infections that are susceptible. It is recognized as the most commonly utilized

N. Meksi et al. (Eds.): ICACE 2024, SPM 97, pp. 57–62, 2025.
https://doi.org/10.1007/978-981-95-4188-1_8

antibiotic worldwide, especially in pediatric cases, owing to its efficient absorption rate and cost-effectiveness. The substantial excretion of these antibiotics in unmetabolized forms by the human body leads to their accumulation [2]. Adsorption is one of the important methods for removing pollutants emerged in water and serves as the foundation for commercially accessible filters. The widespread acceptance of this technique can be attributed to its simplicity and the use of easily obtainable materials.[3].

Response Surface Methodology (RSM) evaluates the associations between the response(s) and the independent variables and elucidates the impact of the independent variables, either individually or collectively, in the various processes. This approach offers numerous benefits such as cost-effectiveness, reduced experimentation requirements, examination of parameter interactions on the response, prediction of responses, assessment of method adequacy, and time efficiency.[4] This technique utilizes low-order polynomial equations within a specified range of independent variables, which are then examined to identify the optimal values of independent variables for optimal responses. The exploration of heavy metal ions adsorption through RSM has garnered particular significance.[5].

This study is predominantly centered on providing valuable perspectives and enhancing the advancement of sustainable water treatment methods, specifically targeting the removal of antibiotic contaminants in a liquid environment, using carbon material modified with phosphoric acid (SC-PPSAC). Additionally, an analysis has been conducted on the impact of different variables, such as pH, concentration of antibiotics, duration of contact, and mass of the adsorbent, on the process of adsorption.

2 Material and Methods

2.1 Batch Adsorption Experiments

Batch adsorption experiments were conducted to investigate the removal of AMX by SC-PPSAC in 30 mL glass flasks. A quantity of 20–400 mg of SC-PPSAC was introduced into 20 mL of AMX solution with concentrations ranging from 50 to 800 mg/L (C_0). The pH of the solution was controlled by additions of 0.1 M HCl and 0.1 M NaOH. The glass flasks were sealed with plastic paraffin film and placed on a shaker at a consistent temperature 30 ± 2 °C, agitated at 150 rpm for a duration of 180 min. Upon reaching equilibrium and separating the sorbent from the solution, the AMX content in the remaining solutions was determined using a spectrophotometer (CECIL-CE 2021). The adsorption capacity of copper ions on LECA (Q_e) was then calculated utilizing a specific equation [6].

$$\boldsymbol{Q_e} = \frac{(\boldsymbol{C_0} - \boldsymbol{C_e})\boldsymbol{V}}{\boldsymbol{m}} \tag{1}$$

where the amoxicillin uptake (mg AMX/g of sorbent) is represented by the variable Q_e, where C_0 and C_e denote the initial and final concentrations of AMX in the solution (mg/L), respectively. V indicates the total volume of the solution (mL), while m indicates the amount of the sorbent used (mg).

2.2 Response Surface Methodology (RSM)

The traditional approach involves the alteration of a single variable while keeping all other parameters constant. The implementation of experiments through this conventional technique, as well as the examination of parameter interactions, is notably time-consuming and impractical. Response Surface Methodology (RSM) stands as a primary constituent of experimental design, facilitating the assessment of various factors and their interplay on system response [7]. This method integrates mathematical and statistical approaches. RSM finds significant application in scenarios where numerous variables influence system response. Notably, RSM comprises three fundamental stages: experiment design, response surface modeling, and optimization. For the present study, the Box-Behnken design (BBD) was chosen and carried out with Minitab 19 statistical software.

3 Results and Discussions

3.1 Effect of Adsorbent Dose

The investigation on dose effect covered a spectrum of SC-PPSAC masses, ranging from 20 to 400 mg in 20 mL of amoxicillin solution with an initial concentration C_0 of 50 mg/L. The outcomes are illustrated in (Fig. 1). With the increase in SC-PPSAC mass from 20 mg to 400 mg, the adsorbed quantity of amoxicillin decreased, ultimately reaching 2.4 mg /g with a yield of 95.31%.

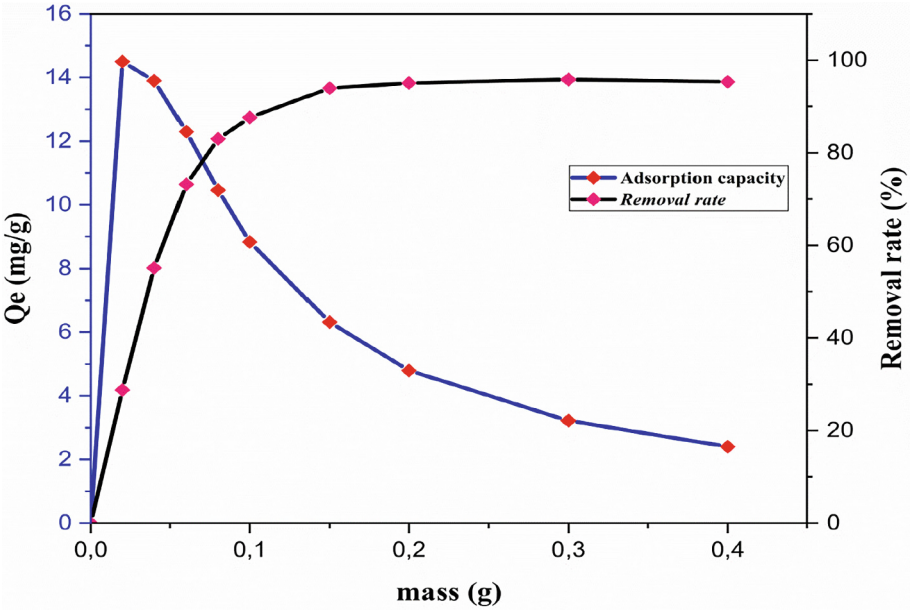

Fig. 1. The effect of adsorbent dose on AMX adsorption capacity and removal rate

3.2 Effect of Contact Time

The duration of contact is a crucial factor affecting the adsorption capacity. The diagram depicted in Figure 8 illustrates how the adsorption capacity of AMX changes with contact time. It is evident that the adsorption of AMX on SC-PPSAC was rapid within the first 20 min. Subsequently, between 20 and 90 min, there was a gradual decrease in the rate of AMX adsorption until equilibrium was reached at 120 min. Thus, 120 min was identified as the time at which equilibrium was achieved (Fig. 2).

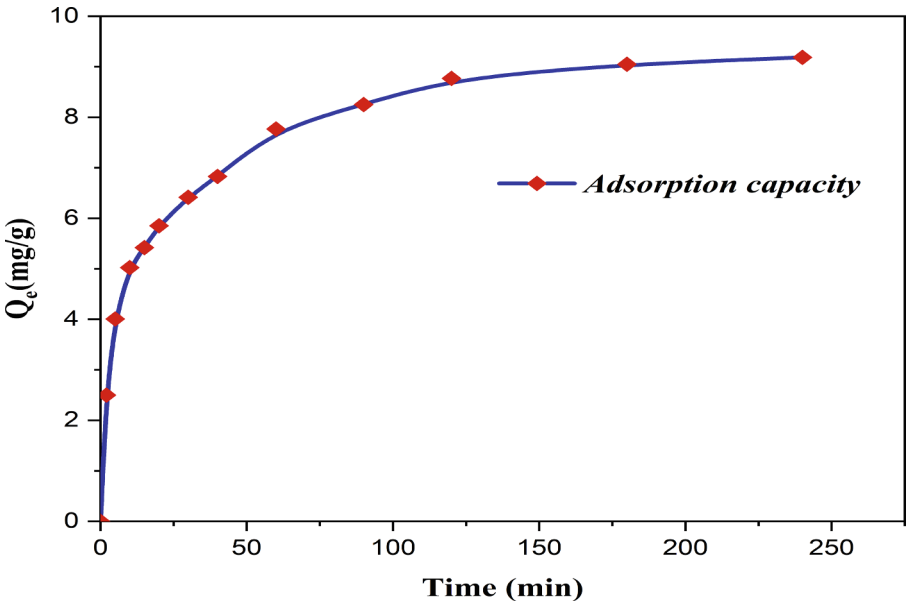

Fig. 2. The effect of contact time on AMX adsorption capacity

3.3 The Design of Experiments for Conducting Studies on Adsorption

The selection of the initial concentration of AMX, time, pH, and adsorbent dose as independent variables was based on prior experimentation. The adsorption capacity of AMX (Q_e) was designated as the response variable for the experiments. The experimental runs were carried out in a random order across three levels. A total of twenty-seven runs were established for the experimental design. To account for pure error, the central point was replicated three times. An analysis of the response was conducted to assess the AMX adsorption performance. The variables were coded at low (−1), middle (0), and high (+1) levels as reported in Table 1, along with the experimental design determining the factors.

Table 1. Variables and their levels

Levels	Mass (g)	C_0 (mg/L)	Time (min)	pH
-1	0.05	50	20	3
0	0.1	100	70	7
+ 1	0.15	150	120	11

In order to better understand the adsorption process of AMX, the three-dimensional response surface plots were analyzed. In each plot, the effects of two factors on the AMX adsorption capacity were investigated when other factors were kept at the optimal value. Figure 3 shows the simultaneous effects of time and pH on the AMX adsorption capacity.

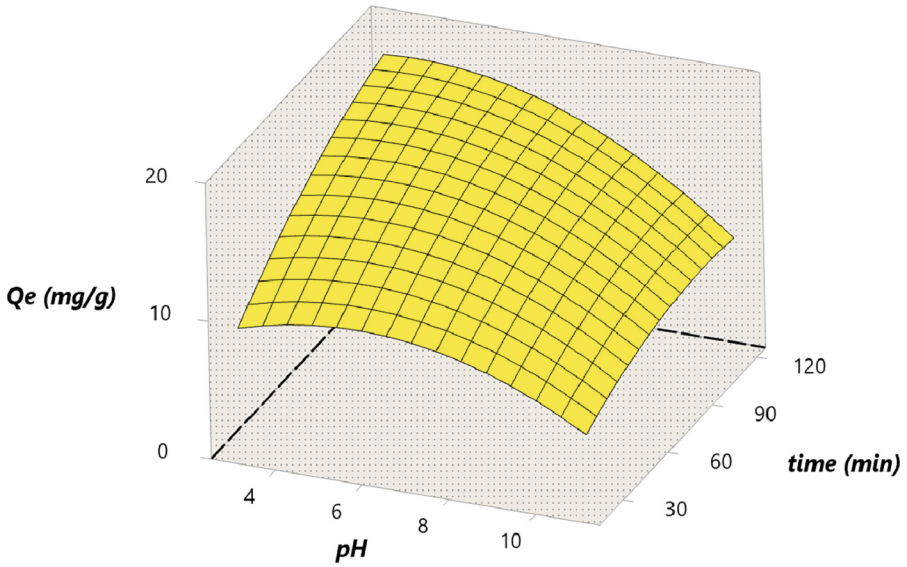

Fig. 3. pH and contact time adsorbent dosage on AMX adsorption capacity

4 Conclusion

The current study is centered on the utilization of Box-Behnken experimental design approach to optimize the process parameters for the elimination of AMX from an aqueous solution using SC-PPSAC. It is observed from batch experimental data that the maximum adsorption capacity of SBAC, reaching approximately 17 mg/g, is obtained under the optimal conditions (m = 0.1 g, C_0 = 140 mg/L, t = 120 min, and pH = 3).

References

1. El Farissi, H., Beraich, A., Lamsayah, M., Talhaoui, A., El Bachiri, A.: The efficiency of carbon modified by phosphoric acid (H3PO4) used in the removal of two antibiotics amoxicillin and

metronidazole from polluted water: experimental and theoretical investigation. J. Mol. Liq. **391**, 123237 (2023). https://doi.org/10.1016/j.molliq.2023.123237
2. Touijer, A., Yahia, E.H., Saidi, M., Taouil, H., Allaoui, M., Ahmed, S.I.: Removal of amoxicillin from an aqueous solution by activated carbon prepared from biomass. J. Ecol. Eng. **24**, 63–79 (2023). https://doi.org/10.12911/22998993/168350
3. Moussavi, G., Alahabadi, A., Yaghmaeian, K., Eskandari, M.: Preparation, characterization and adsorption potential of the NH4Cl-induced activated carbon for the removal of amoxicillin antibiotic from water. Chem. Eng. J. **217**, 119–128 (2013). https://doi.org/10.1016/j.cej.2012.11.069
4. Yetilmezsoy, K., Demirel, S., Vanderbei, R.J.: Response surface modeling of Pb(II) removal from aqueous solution by Pistacia vera L.: box–behnken experimental design. J. Hazard. Mater. **171**, 551–562 (2009). https://doi.org/10.1016/j.jhazmat.2009.06.035
5. Shojaeimehr, T., Rahimpour, F., Khadivi, M.A., Sadeghi, M.: A modeling study by response surface methodology (RSM) and artificial neural network (ANN) on Cu2+ adsorption optimization using light expended clay aggregate (LECA). J. Ind. Eng. Chem. **20**, 870–880 (2014). https://doi.org/10.1016/j.jiec.2013.06.017
6. Ayeb, A., Binous, H., Dhaouadi, H., Dridi-Dhaouadi, S.: Commercial dimethoate pesticide adsorption on organic soil: experimental and theoretical investigations. Chemistry Africa. **7**, 5521–5534 (2024). https://doi.org/10.1007/s42250-024-01106-x
7. Bouatay, F., Eljebsi, N., Dridi-Dhaouadi, S., Mhenni, F.: Valorization of the Vicia faba mucilage on textile wastewater treatment as a bio-flocculant: process development and optimization using response surface methodology (RSM). Water Sci. Technol. **75**, 629–642 (2017). https://doi.org/10.2166/wst.2016.480

Assessment of Iron Contamination in Groundwater of Catchment Area Water in Nakatt from Kiffa (Mauritania)

Aichetou Brahim Boutebib[1,2,3](✉), Abdoulaye Demba N'diaye[1,2,3], Oumar Mamadou Sy[1,2,3], Sid' Ahmed Baba Elhoumed[1,2,3], Bocar Kalidou M'Baye[1,2,3], and Bakari Mohamed Semega[1,2,3]

[1] Unité de Recherche, Eau Pollution et Environnement, Département de Chimie, Faculté Des Sciences et Techniques, Université de Nouakchott, Nouakchott, Mauritanie
[2] Service Laboratoire, Cellule Management Qualité, Société Nationale d'Eau (SNDE), Nouakchott, Mauritanie
[3] Laboratoire de Chimie, Institut National de Recherches en Santé Publique, Nouakchott, Mauritanie

Abstract. This study investigates the occurrence of iron (Fe) in the catchment area water in Nakatt from Kiffa in Mauritania. The study area was monitored during January and August. The occurrence of Fe in the groundwater showed significant spatial and temporal fluctuations. The relationship between Fe and some physicochemical parameters was also analyzed statistically using Pearson's correlation matrix. Firstly, the results suggested that the concentration of Fe was influenced by the dissolution of Fe minerals. Secondly, the results show that the pH value was an important factor that influenced the Fe concentrations in the groundwater. The Water Quality Index (WQI) and Comprehensive Pollution Index (CPI) method was used to evaluate the suitability for human consumption. The results show that WQI and CPI are strongly influenced by Fe indicating that Fe removal would contribute to excellent well water. However, CPI also shows that the pH is a parameter to be optimized for possible potabilization. From the result of the present study, it is highly recommended that different treatment techniques should be employed to purify groundwater before consumption.

Keywords: groundwater · iron · Kiffa · Mauritania

1 Introduction

Groundwater is one of the primary freshwater sources for drinking, irrigation, and industrial uses in most communities worldwide [1]. However, the quality of global water has rapidly declined for decades due to the impact of both natural and anthropogenic factors [2]. Some chemicals might produce immediate impacts on human health because of the nature of the hazardous chemicals [3]. Severe human health implications are associated with heavy metal exposure. Among the heavy metal, Fe is a fairly abundant element in rocks and is found in the form of silicates, oxides as well as hydroxides, carbonates and

N. Meksi et al. (Eds.): ICACE 2024, SPM 97, pp. 63–74, 2025.
https://doi.org/10.1007/978-981-95-4188-1_9

sulfides [4]. Drink of water containing Fe at concentrations 3 mg/L or higher for a long time causes hemochromatosis and other effects [5]. At the same time, the oxidation of Fe makes water turbid and odorous, and excessive Fe content in groundwater also causes pipeline rust and blockage of wells [6].

Encouraging results obtained by assessment of Fe contamination in groundwater of catchment area water from Derwiche in Mauritania [7] have incited us to search new route to study the catchment area water from Nakatt in Mauritania. The present study aims to investigate the contamination levels of Fe in the groundwater in catchment area water in Nakatt from Kiffa in Mauritania. Assessing water quality is an important strategy for food safety and human health.

2 Materials and Methods

2.1 Description of the Study Area

Assaba is the third region in the administrative classification of Mauritania. The Wilaya of Assaba is located in south-central Mauritania and occupies an area of 36,600 km^2. Its capital is Kiffa (Fig. 1), the second largest Mauritanian city in population. Assaba is an agropastoral zone par excellence. The boreholes are located in the Kiffa city watershed at the level of the pumping station (Nakatt). The selected boreholes were F2, F14Bis, and F15. These boreholes are located at about 30 km from Kiffa. It is important to note that there is no industrial production and agricultural activities in the study area.

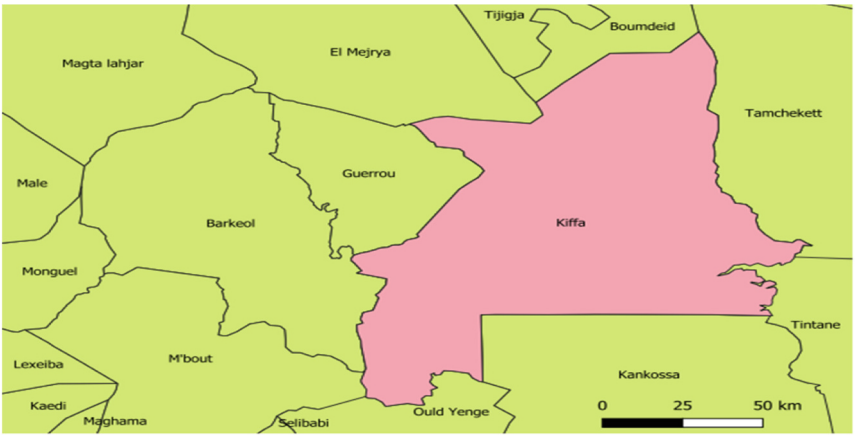

Fig. 1. Kiffa localisation

2.2 Sampling Procedures and Physicochemical Parameters

Water samples were collected from three sampling sites (Boreholes) scattered along the catchment area water in Nakatt from Kiffa. The samples were collected two times: the first sampling was done in January and the last in August corresponding to the rainy period. The sampling for the analysis of physico-chemical parameters was carried

out at the selected site, using a 1.5 L polyethylene bottle. The collected samples were stored at 4 °C in insulated boxes and transported to the laboratory. Equipment used for measurement of physicochemical parameters such as temperature, pH, Electrical Conductivity (EC), Total Dissolved Solids (TDS), nitrates (NO_3^-), Sulphates (SO_4^{2-}), chlorides (Cl^-), oxidizability (organics mattes: OM), and iron (Fe), are listed in Table 1.

Table 1. Water quality parameters and measurement methods

Parameter	Unit	Measuring equipment and method analysis
Temperature	°C	pH meter
pH		pH meter HI 991001
EC	µS/cm	conductimeter HI98192
TDS	mg/L	conductimeter HI98192
Cl^-	mg/L	Volumetric dosage with Silver nitrate
NO_3^-	mg/L	Photometer Wagtech 7100
SO_4^{2-}	mg/L	Photometer Wagtech 7100
OM	mg/L	Hot oxidation in an acid medium by potassium permanganate
Fe	mg/L	Photometer Wagtech 7100

2.3 Calculation of Water Quality Index (WQI)

The determined WQI values are classified into five classes as mentioned by Ramakrishnaiah et al. [8]. In this study the WQI for drinking purposes is considered and permissible WQI for the drinking water is taken as:

$$WQI = \frac{\sum_{i=1}^{n} q_i w_i}{\sum_{i=1}^{n} w_i}$$

The determined WQI values are classified into five classes as mentioned in Table 2.

Table 2. The WQI categories

Range	Quality
<50	Excellent water
50-100	Good water
100-200	Poor water
200-300	Very poor water
>300	Unsuitable for drinking

2.4 Comprehensive Pollution Index (CPI)

The CPI is classified into five categories as mentioned by Son et al, (2020) [9]. The formula to calculate CPI is presented as follows:

$$CPI = \frac{1}{n}\sum_{i=1}^{n} PI_i$$

where CPI = Comprehensive Polluted Index; n = number of monitoring parameters; PIi = the pollution index number i. PIi is calculated according to the following equation:

$$PI = \frac{C_i}{S_i}$$

$$PI = \frac{C_i}{S_i}$$

where C_i = measured concentration of parameter number in water; S_i = permitted limitation of parameter number according to environmental standard. CPI is classified into five categories as mentionned in Table 3:

Table 3. The CPI categories

Category	PCI	Classification
1	0–0,20	clean
2	0,21–0,40	Sub clean
3	0,41–1	Slightly polluted
4	1,01–2	Medium polluted
5	≥2,01	Heavily polluted

3 Results and Discussions

3.1 Physicochemical Parameters

The physicochemical parameters such as Temperature, pH, EC, TDS, SO_4^{2-}, NO_3^-, Cl^-, OM and Fe studied in the catchment area water in Nakatt during January and August were represented in Figs. 2, 3, 4, 5, 6, 7, 8, 9 and 10. These physicochemical parameters were evaluated according to standard limits of the WHO (2011) for drinking water [10].

Temperature values ranged from 27.2 °C to 28 °C in January and from 28.4 °C to 29 °C in August (Fig. 2). The temperature values recorded in groundwater in this study were similar to a study conducted by Ojekunle et al., [11], who reported temperature ranges of 28 °C to 30 °C in groundwater of an industrial area in Nigeria. The pH values during the January ranges from 6.86 to 7.32. However the pH values of August ranges from 7.01 to 7.66 (Fig. 3). The observed pH values recorded in the January were slightly

acidic. Consumption of acidic water, as observed in the analysed groundwater can lead to corrosion of water pipes and may have potential health effect on receptors when consumed. This may also lead to negative effect on gastrointestinal tract which has potential to result in diarrhea [12]. Similarly, acidic water has been attributed irritation of skin and eye, mucous membrane cell damage [13].

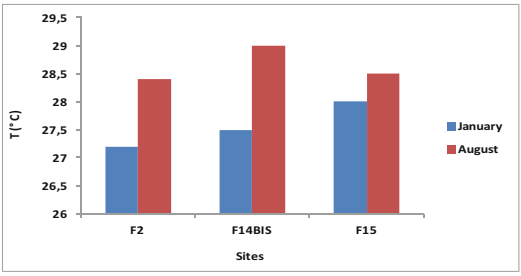

Fig. 2. Spatio-temporal variation of Temperature

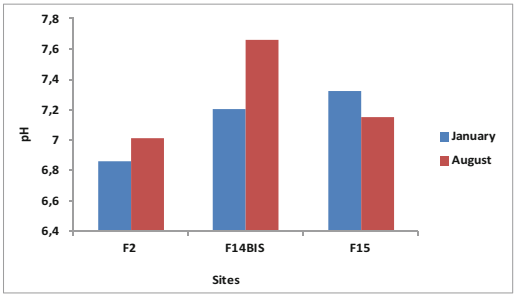

Fig. 3. Spatio-temporal variation of pH

EC measures the presence of ions in water. EC values vary within a range of 79–109 µS/cm in January and 122.5–182.5 µS/cm in August (Fig. 4). TDS is a measure of inorganic salts. The TDS values vary within a range of 40–54 mg/L in January and 48.6–70.2 mg/L in August (Fig. 5).

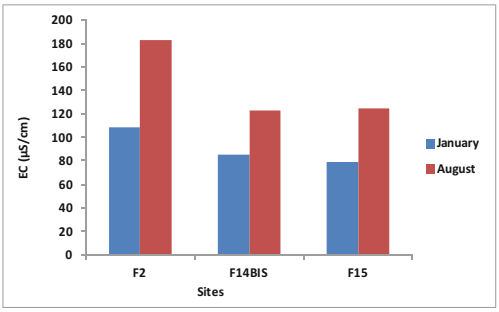

Fig. 4. Spatio-temporal variation of EC

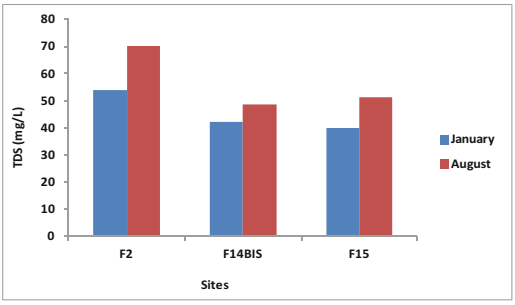

Fig. 5. Spatio-temporal variation of TDS

Chlorides values vary within a range of 17.75–21.3 mg/L in January and 21.3–28.4 mg/L in August (Fig. 6). The observed concentration of chloride ion in groundwater under consideration falls below the acceptable level of 200 mg/L [10]. However, no adverse health effects on human being have been reported by the consumption of water having excess concentration of chloride [14].

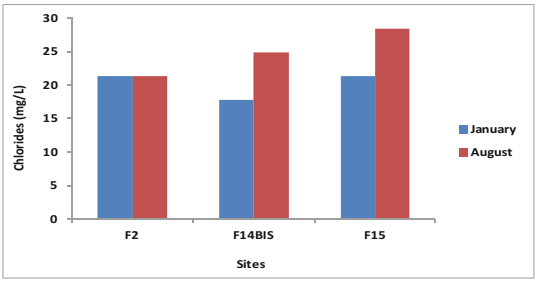

Fig. 6. Spatio-temporal variation of Chlorides

Nitrates values vary within a range of 2.4–15.2 mg/L in January and 1.1–1.3 mg/L in August (Fig. 7). Sulphates values vary within a range of 21–59 mg/L in January and 28–50 mg/L in August (Fig. 8).

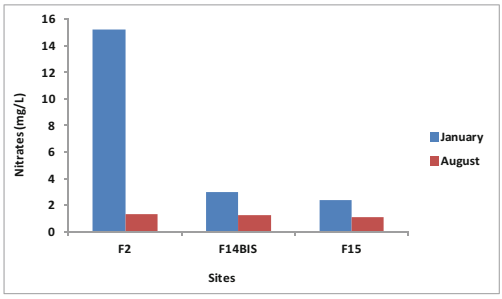

Fig. 7. Spatio-temporal variation of nitrates

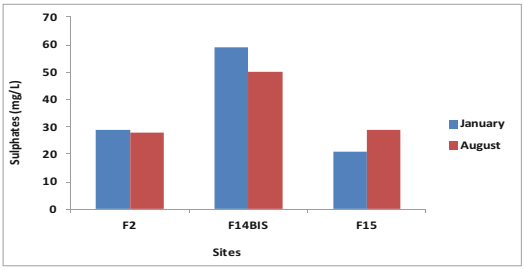

Fig. 8. Spatio-temporal variation of sulphates

OM values vary within a range of 0.64–1.28 mg/L in January and 1.2–1.98 mg/L in August (Fig. 9). It is observed that the OM contents show very high values in August. The Temperature, pH, EC, TDS, SO_4^{2-}, NO_3^{-}, Cl^{-}, and OM contents of water samples are within WHO for drinking water [10].

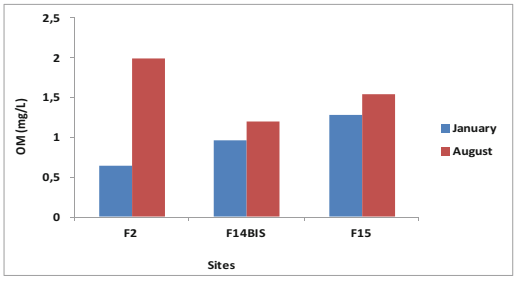

Fig. 9. Spatio-temporal variation of OM

3.2 Spatio-Temporal Variation of Fe

Fe values vary within a range of 15.7–38.4 mg/L in January and 9-10 mg/L in August (Fig. 10). It is observed that the Fe contents show very high values in January. The decrease in Fe in August probably due to the dilution effect of rain water. The limiting Fe concentration is set at 0.3 mg/L [10].

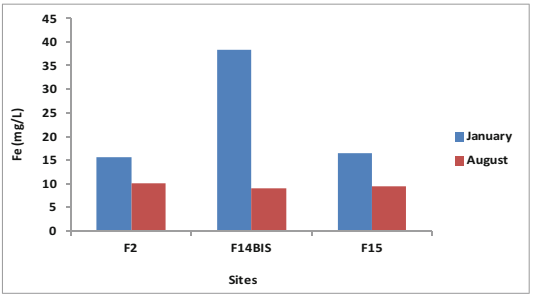

Fig. 10. Spatio-temporal variation of Fe

3.3 Pearson Correlation Analysis

The degree estimated by Pearson's connection coefficients for the January and August in catchment area water in Nakatt from Kiffa is exhibited in Tables 4 and 5, respectively.

From the Table 4, highly significant correlation were found between Fe and SO_4^{2-} ($r = 0.973$). Positive correlation coefficient Fe and pH ($r = 0.458$), except betwen Fe and Cl^- ($r = -1$), Fe and NO_3^- ($r = -0.491$), Fe and TDS ($r = -0.410$) and Fe and EC ($r = -0.357$).

According to Table 5, the highly significant correlation were found between Fe and OM ($r = 0.997$), Fe and TDS ($r = 0.918$) and Fe and EC ($r = 0.880$). Positive correlation coefficient Fe and NO_3^- ($r = 0.500$), except betwen Fe and pH($r = -0.950$), Fe and SO_4^{2-} ($r = -0.885$) and Fe and Cl^- ($r = -0.500$).

Table 4. Pearson-correlation matrix in catchment area water in Nakatt from Kiffa during january

Variables	Fe	pH	EC	TDS	Cl^-	SO_4^{2-}	NO_3^-	OM
Fe	**1**			.				
pH	0,296	**1**						
EC	−0,357	−0,998	**1**					
TDS	−0,410	−0,993	0,998	**1**				
Cl^-	−1,000	−0,266	0,327	0,381	**1**			
SO_4^{2-}	0,973	0,068	−0,132	−0,189	−0,980	**1**		
NO_3^-	−0,491	−0,977	0,989	0,996	0,464	−0,277	**1**	
OM	0,031	0,964	−0,945	−0,924	0,000	−0,200	−0,886	**1**

Table 5. Pearson-correlation matrix in catchment area water in Nakatt from Kiffa during August

Variables	Fe	pH	EC	TDS	Cl-	SO_4^{2-}	NO_3^-	OM
Fe	**1**							
pH	−0,950	**1**						
EC	0,880	−0,687	**1**					
TDS	0,918	−0,748	0,996	**1**				
Cl^-	−0,500	0,205	−0,852	−0,803	**1**			
SO_4^{2-}	−0,885	0,986	−0,558	−0,628	0,040	**1**		
NO_3^-	0,500	−0,205	0,852	0,803	−1,000	−0,040	**1**	
OM	0,997	−0,921	0,916	0,947	−0,569	−0,844	0,569	**1**

The strong and negative correlation was found between Fe – pH ($r = -0.950$) (Table 4) during August. This mean that if the value of pH increases, then the concentration of Fe will decrease or vice versa. The observed pH values recorded in the january were slightly acidic than the pH values in August. According to Harvey and Fuller [15], a decrease in pH will accelerate the dissolution of carbonates and hydroxides. These results could confirm the high Fe level recorded in january. However, the decrease in Fe in August probably due to the dilution effect of rain water.

The strong and positive correlation was found between Fe–TDS ($r = 0.918$) and Fe – EC ($r = 0.880$) (Tables 5) during august. According to Akbar et al., (2020) [16], the strong and positive correlation obtained between Fe–TDS and Fe – EC suggested that the concentration of Fe was influenced by dissolution minerals in groundwater. However, it is important to note a negative and significative correlations between Fe andTDS ($r = -0.410$) and Fe and EC ($r = -0.357$) (Table 5) were obtained during January. These results showed that the catchment area water in Nakatt well was influenced by dissolution minerals in groundwater during the rainy period.

The higher Fe concentrations obtained in catchment area water in Nakatt during January might have been the results of interaction of underground oxidized iron minerals with OM present. In addition, the observed slightly acidic pH values recorded in the January can accelerate the dissolution of Fe_2CO_3 present in rocks. Similar observations are reported by Mondal et al. [17]. Similarly, a decrease in pH will accelerate the dissolution of carbonates and hydroxides. Fe bound to carbonates will be released into the water [15].

The strong and positive correlation was found between Fe-OM ($r = 0.997$) during August (Table 5). It is observed that the OM contents show very high values in August. However, the decrease in Fe in August probably due to the dilution effect of rain water.

3.4 Assessment of the Water Quality Using WQI

When Fe studied are included in the calculation of the WQI for the catchment area water in Nakatt from Kiffa (Table 6), all values of WQI are higher than 300 which means that the water is unsuitable for drinking. However, without including Fe (Table 7), all values are lower than 50 which mean that the water is excellent for drinking.

Table 6. WQI values for all parameters

Sites	January	Quality	August	Quality
F2	4742.97	Unsuitable for drinking	3023.63	Unsuitable for drinking
F14Bis	3150.53	Unsuitable for drinking	2721.15	Unsuitable for drinking
F15	4985.20	Unsuitable for drinking	2872.26	Unsuitable for drinking

Table 7. WQI values without including Fe

Sites	January	Quality	August	Quality
F2	36.70	Excellent water	49.24	Excellent water
F14Bis	40.51	Excellent water	44.91	Excellent water
F15	44.45	Excellent water	46.66	Excellent water

3.5 Assessment of the Water Quality Using CPI

When Fe studied is included (Table 8) in the calculation of the CPI for the in catchment area water in Nakatt from Kiffa all values of CPI are higher than 2.01 which means that the water is heavily polluted. Without including Fe (Table 9), all values of CPI are between 0.21 and 0.40 which means that the water is sub clean. However, without including Fe and pH (Table 10), all values of CPI are between 0.21 and 0.40 which means that the water is clean.

Table 8. CPI values for all parameters

Sites	June	Quality	August	Quality
F2	7.70	Heavily polluted	4.99	Heavily polluted
F14Bis	18.50	Heavily polluted	4.51	Heavily polluted
F15	8.06	Heavily polluted	4.74	Heavily polluted

Table 9. CPI values without including Fe

Sites	June	Quality	August	Quality
F2	0.26	Sub clean	0.26	Sub clean
F14Bis	0.25	Sub clean	0.26	Sub clean
F15	0.23	Sub clean	0.25	Sub clean

Table 10. CPI values without including Fe and pH

Sites	June	Quality	August	Quality
F2	0.15	Sub clean	0.15	Clean
F14Bis	0.13	Sub clean	0.13	Clean
F15	0.11	Sub clean	0.13	Clean

4 Conclusions

This study investigates the occurrence of Fe in the catchment area water in Nakatt from Kiffa city in Mauritania. The occurrence of Fe in the groundwater showed significant spatial and temporal variations. The relationship between Fe and some physicochemical parameters was also analysed statistically using Pearson's correlation matrix. Firstly, the results suggested that the concentration of Fe was influenced by dissolution iron minerals. Secondly, the results show that the pH value was an important factor that influenced the Fe concentrations in the groundwater. The WQI and CPI are used to identify influence of the Fe contamination. These results indicate that Fe removal would contribute to excellent well water. However, CPI also show that the pH is a parameter to be optimized for possible potabilization. From the result of the present study, it is highly recommended that different treatment techniques should be employed to purify groundwater before consumption.

References

1. Marghade, D., Malpe, D.B., Subba Rao, N.: Applications of geochemical and multivariate statistical approaches for the evaluation of groundwater quality and human health risks in a semi-arid region of eastern Maharashtra, India. Environ. Geochem. Health. **43**, 683–703 (2021)
2. Vadde, K.K., Jianjun, W., Long, C., Tianma, Y., Alan, J., Raju, S.: Assessment of water quality and identification of pollution rick locations in Tiaoxi river (Taihu watershed), China. Water **10**, 183 (2018)
3. Alemu, Z.A., Teklu, K.T., Alemayehu, T.A., Balcha, K.H., Mengesha, S.D.: Physicochemical quality of drinking water sources in Ethiopia and its health impact: a retrospective study. Environ. Syst. Res. **4**, 22 (2015)
4. Zhang, Z., Xiao, C., Adeyeye, O., Yang, W., Liang, X.: Source and mobilization mechanism of iron, manganese and arsenic in groundwater of Shuangliao City. Northeast China Water **12**(2), 534 (2020)
5. Weng, H., Qin, Y., Chen, X.: Elevated iron and manganese concentrations in groundwater derived from the Holocene transgression in the Hang-Jia-Hu Plain. China Hydrogeol. J. **15**, 715–726 (2007)
6. Ye, X., Cui, R., Wang, L., Du, X.: The influence of riverbank filtration on regional water resources: a case study in the second Songhua River Catchment, China. Water Sci. Tech. Water Supply **20**, 1425–1438 (2020)

7. Boutebib, A.B., et al.: Assessment of iron contamination in groundwater of catchment area water. Indon. J. Sci. Technol. **8**(3), 429–438 (2023)
8. Ramakrishnaiah, C.R., Sadashivaiah, C., Ranganna, G.: Assessment of water quality index for the groundwater in Tumkur Taluk, Karnataka state, India. E-J. Chem. **6**(2), 523–530 (2009)
9. Son, C.T., Giang, N.T.H., Thao, T. P., Nui, N.H., Lam, N.T., Cong, V.H.: Assessment of Cau River water quality assessment using a combination of water quality and pollution indices. J. Water Supply: Res. Technol.—AQUA **69**(2), 160–172 (2020)
10. WHO (World Health Organisation) Guidelines for drinking water quality (4^{th} edition), Geneva, Switzerland (2011)
11. Ojekunle, Z.O., Adeyemi, A.A., Taiwo, A.M., Ganiyu, S.A., Balogun, M.A.: Assessment of physicochemical characteristics of groundwater within selected industrial areas in Ogun State, Nigeria. Environ. Pollut. Bioavailabil. **32**(1), 100–113 (2020). https://doi.org/10.1080/26395940.2020.1780157
12. Obiefuna, G.I., Sheriff, A.: Assessment of shallow ground water quality of Pindig Gombe Area, Yola Area, NE, Nigeria for irrigation and domestic purposes. Res. J. Environ. Earth Sci. **3**(2), 131 (2011)
13. Meinhardt, P.L.: Recognizing waterborne disease and the health effects of water contamination: a review of the challenges facing the medical community in the United States. J. Water Health **4**(S1), 27–34 (2006)
14. Jain, C.K., Bandyopadhyay, A., Bhadra, A.: Assessment of ground water quality for drinking purpose, District Nainital, Uttarakhand, India. Environ. Monit. Assess. **166**(1–4), 663–676 (2010)
15. Harvey, J., Fuller, C.: Effect of enhanced manganese oxidation in the hyporheic zone on basin-scale geochemical mass balance. Water Res. Res. **34**, 623–636 (1998)
16. Akbar, N.A., et al.: Characteristic of groundwater well quality using bivariate analysis: a case study at USM Engineering Campus, Penang. IOP Conf. Ser.: Earth Environ. Sci. **646**, 012060 (2021). https://doi.org/10.1088/1755-1315/646/1/012060
17. Mondal, N.C., Singh, V.S., Puranik, S.C., Singh, V.P.: Trace element concentration in groundwater of Pesarlanka island, Krishna delta India. Environ. Monit. Assess. **163**, 215–227 (2010)

Author Index

N. Meksi et al. (Eds.): ICACE 2024, SPM 97, p. 75, 2025.
https://doi.org/10.1007/978-981-95-4188-1